UNIVERSITY OF SOUTHAMPTON

DEPARTMENT OF SHIP SCIENCE

FACULTY OF ENGINEERING

AND APPLIED SCIENCE

METHODS TO DETERMINE THE BEHAVIOUR OF A
FERROCEMENT PANEL

D.R. Prentice

August 1979

Ship Science Report No. 4/78

METHODS TO DETERMINE THE BEHAVIOUR

OF A FERROCEMENT PANEL

by

D. R. Prentice

Ship Science Report 4/78

The Basis for this report is :

"AN INVESTIGATION INTO THE APPLICATION OF CLASSICAL
PLATE THEORIES TO THE BEHAVIOUR OF A FERROCEMENT PANEL"
D. R. Prentice, B.Sc. Hons. Report, Ship Science,
Southampton University, 1979.

ACKNOWLEDGEMENTS

The Author wishes to express his thanks to the following who have contributed to the production of this report;

LIST OF SYMBOLS

a	Width of panel between support hinges
A_s	Cross-sectional area of reinforcement wire per unit width
$d_1, d_2, \ldots$	Distances of the reinforcement layers from the tension surface of the panel
d_c	Depth of the initial crack in the 'uncracked section'
d_n	Distance of the neutral axis from the tension surface of the panel
E_c, E_s	Young's Moduli of Elasticity; concrete, steel
f'_c	Uniaxial compressive strength of concrete
f_{cu}	Cube strength of concrete
f'_{ct}	Modulus of Rupture of concrete
G	Shear Modulus of Elasticity
I_x, I_y	Second Moment of area in O_x, O_y directions
I_u	Second moment of area of the uncracked section
I_c	Second moment of area of the cracked section
k_i, k'_i	Deflection coefficients for isotropic and orthotropic theory
k_2	Strain coefficient for isotropic theory
K_x	Coefficient of coverage
m, m_c, m_s	Mass; of concrete, steel
M, M_x, M_y	Moments per unit width
M_u	Limit-state moment per unit width
P_s, P_c	Forces in panel per unit width; steel, concrete
R	Radius of curvature of panel element in bending
t	Panel thickness
u, v, w	Displacements in the principal directions of the $Oxyz$ axes set
x, y, z	Rectangular Cartesian co-ordinates
U	Strain energy
γ_m	Partial Safety Factor
δ	Deflection of panel in Oz direction
ϵ, ϵ_i	Direct strain components
λ	Constants
ν	Poisson's Ratio
ρ, ρ_s, ρ_c	Density; concrete, steel
σ	Direct Stress

Σ	Summation
θ, ϕ	Angles between axes set directions

INDEX

1.0 INTRODUCTION

Ferrocement is a form of reinforced concrete. It consists basically of a matrix of concrete with a high proportion of steel reinforcement in the form of wiremesh.

Although ferrocement appears, from its use in the construction of vessels since World War II, to be a relatively new material it was in fact first used in this way in 1847 by Jeanne-Pierré Lambot. The history of ferrocement as described in Reference 1 reflects the usual situation encountered by a new material of a misunderstanding and over expectation of its properties. More recently there was a 'boom period' of activity in the sixties and early seventies which has now subsided. Many amateur boatbuilders met with constructional and economic difficulties associated with rising completion costs. For the yachtsman, the attraction of a cheap hull has been limited to cruising vessels since ferrocement is heavy compared with equivalent GRP and aluminium designs. Nevertheless, it may be that vessels have been too heavy because of overbuilding since very few vessels have been lost due to hull failure. Since the hull cost represents 30 - 40% of the total cost, any small savings here are almost insignificant for the yachtsman. However the continuing rise of crude oil price may see an increase in cost of GRP thus making ferrocement relatively more attractive.

Ferrocement is attractive for many other marine applications. In the developing countries of the world working boats, especially fishing craft, have been built successfully. Low labour costs as well as minimal material costs are key advantages as well as the basic material properties. Ferrocement is durable, non corroding in tropical environments, fireproof, rot proof, easily formed, has good resistance to impact damage and is easily repaired.

1.1 The Behaviour of Ferrocement Panels

The problem of the prediction of the deflection of a ferrocement panel under a lateral loading concerns the properties of the steel and concrete components, their relative proportion and the geometry of the panel. Basically with increasing deformation a section of the panel will pass through 3 phases. Initially the section is called 'uncracked' and the concrete resists both tensile and compressive stresses. With increasing deformation the concrete

in tension cracks because of the low tensile strength of concrete and the section is then called 'cracked'. The stiffness of the cracked section is significantly lower than that of the uncracked section. Finally the section reaches a yielding condition called the 'failure' section.

The problems of a complete analysis of behaviour up to failure will therefore involve a panel with varying properties over its area.

1.2 The Aim of The Report

Investigation has shown that there has only been limited research into the behaviour of ferrocement. Clearly the basic mechanical properties of ferrocement have been determined and it will as yet be a while before service experience highlights the most important problems of ferrocement as a structure for example corrosion, fatigue, constructional restraints etc.

The Naval Architect needs to be able to design to various criteria of performance. In the case of ferrocement watertightness is retained until considerable deformation and cracking is achieved. Thus the prediction of panel deflection is of importance under design loads as well as the ultimate load at failure.

The aim of this report is to bridge the gap between simple specimen tests and the behaviour in practice of what could be over-built structures. The basis for this report is Reference 1 which gives details of the author's work on simply supported ferrocement panels subjected to uniform lateral pressure. In particular the effect of mesh arrangement on behaviour was observed. Reinforced concrete theory in various forms was applied in order to attempt to predict the behaviour.

2.0 A REVIEW OF METHODS AVAILABLE FOR APPLICATION TO FERROCEMENT PANELS

Simple classical plate theory can deal with elastic behaviour of the panel. Failure must be considered separately. Since both the 'uncracked' and cracked sections behave effectively elastically simple elastic plate theory can be extended up to a limit imposed by the effect of membrane action at large deflections. This limit was taken as central deflection equals 0.75 of thickness. The failure pressure must be calculated separately. The limitations of such predictions are shown by the diagram below.

$(\delta = 0.75t)$ Central Deflection
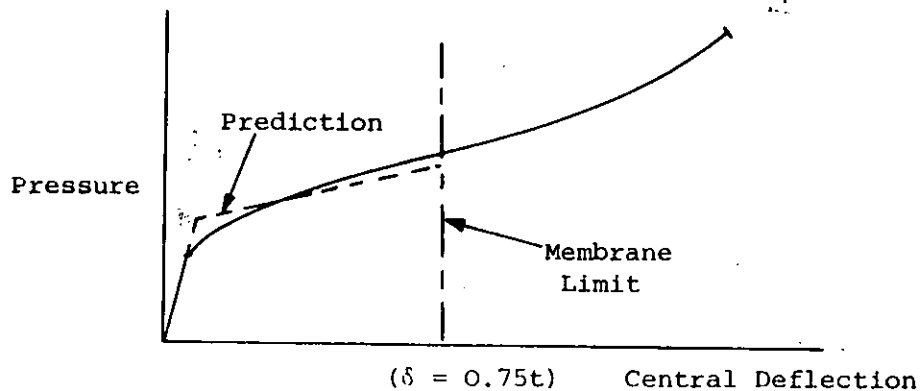
Simple membrane theory is available for a pure membrane, and various complicated solutions to include both bending and membrane action are available from Large deflection theory, but they were not considered in this report.

Classical plate theory includes both isotropic and ortho-tropic theories as compared in section 4. In isotropic behaviour the panel is taken to behave with the same properties in all directions. The various possible arrangements of mesh layers in the panel means that the properties can be significantly different in the orthogonal directions. The effect of the directional properties on the panel as a whole is considered by simple orthotropic plate theory.

The extension of simple classical theory into the cracked region can be considered with relation to the initiation of cracking, thereafter considering the panel fully cracked as described in section 5.2. It was also noted that classical solutions are available to approximate behaviour of panels with different stiffness in different areas and these and their limitations are described in section 5.3.

The ultimate strength of a panel is calculated from "Limit State Theory" as shown in section 6.1.

With the availability of higher computing power the finite difference and finite element methods can be used to construct comprehensive models of the panel under deflection up to failure.

The finite difference solution is a numerical method of approximating the differential terms in the equations governing the equilibrium of the panel and is based on the deflection at points on a grid on the panel. Variable elastic stiffness can be easily considered as can the plastic behaviour of the failure section, but with more difficulty. A more accurate solution is obtained using more grid points. Another attractive feature of this method is that a variety in edge support combinations as well as overall geometry can be considered where classical theory is not easily applied. The major difficulty with the method is to determine the areas of differing stiffness which alter with deflection. Reference 2 gives a comprehensive survey of the method.

The finite element method divides the plate up into a set of elemental sections and considers their equilibrium. In order to define the geometry variables are required at each node in order to express deflection and twist etc. Reference 3 gives a layered model which is able to consider all of the basic properties of steel and concrete and as such probably represents the ultimate solution to this type of problem. It is, however, very expensive in terms of computer time even when compared to the finite difference method.

Finite difference and element methods are beyond the scope of both this report and Reference 1. Thus the remainder of this report will be confined to summarising the simple classical methods available together with the interpretation of the use of the methods.

3.0 TRANSFORMED SECTIONS OF THE UNCRACKED, CRACKED AND
FAILURE PHASES

During the bending of a ferrocement panel the sectional properties can be described by the three phases of the uncracked, cracked and failure sections. In order to calculate the flexural rigidity, 'D', where

$$D = \frac{EI}{1-\nu^2} \qquad (3.1)$$

of the uncracked and cracked sections, they are expressed in terms of an 'I' value for an equivalent steel section. 'I' is the second moment of area per unit width of the section taken about the neutral axis of the section. Thus from simple beam theory the equivalent steel 'I' of the composite section is

$$I = I_s + \frac{E_c}{E_s} I_c \qquad (3.2)$$

Finally a moment of resistance per unit length to bending of the plastic hinge is calculated for the failure section.

3.1 The Final Model for the Uncracked Section

Cross Section   Strain
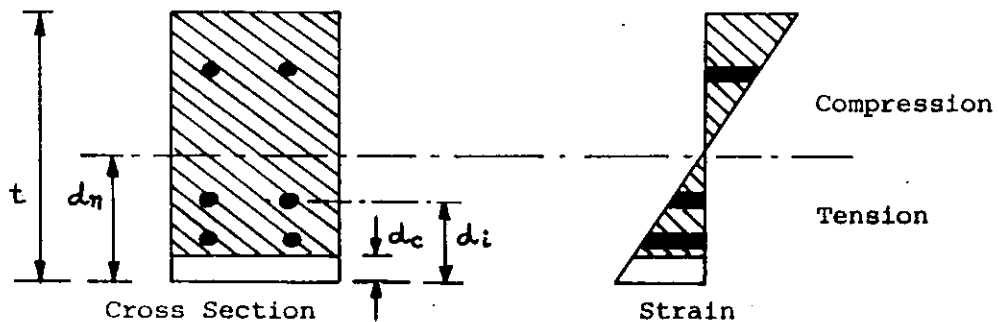
It was found from comparison between experimental results and theory as described in section 4.2 the best model for the uncracked section considers it to be cracked through the covering layer of concrete in the tension surface. Thus for the purpose of constructing a satisfactory model this initial crack depth, d_c, had to be included as shown.

Expressions for the depth of the neutral axis and the equivalent steel 'I' were obtained in Reference 1 using simple beam theory for a perfectly elastic section. Using the notation of the diagram these expressions were

$$d_n = \frac{A_s \left(1 - \frac{E_c}{E_s}\right) \sum_{i=1}^{N} d_i + \frac{1}{2}\frac{E_c}{E_s}(t^2 - d_c^2)}{A_s \left(1 - \frac{E_c}{E_s}\right) N + \frac{E_c}{E_s}(t - d_c)} \qquad (3.3)$$
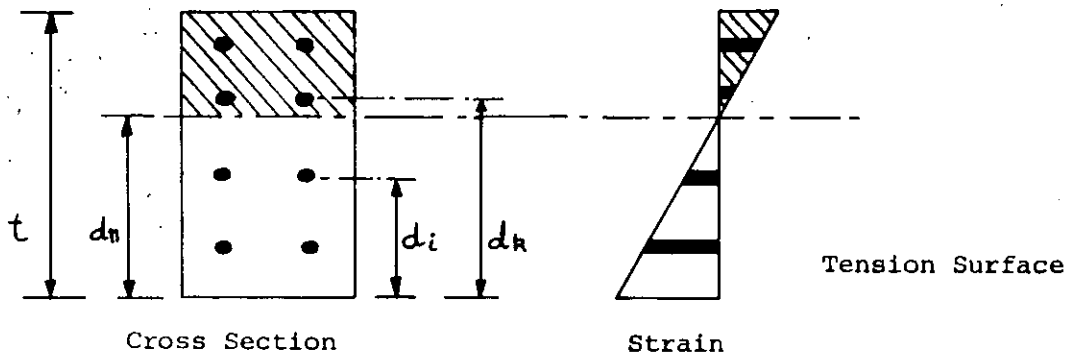
and
$$I_u = A_s \left(1 - \frac{E_s}{E_c}\right) \sum_{i=1}^{N} (d_n - d_i)^2 + \frac{1}{3}\frac{E_c}{E_s}\left[(d_n - d_c)^3 + (t - d_n)^3\right] \quad (3.4)$$

where A_s = area of steel reinforcement per unit width per layer
and N = number of layers of reinforcement.

Calculation is straightforward using equation 3.3 to evaluate d_n and substituting this value into 3.4 to find I_u.

3.2 The Cracked Section

Cross Section   Strain   Tension Surface

In this phase the concrete is assumed cracked up to the neutral axis in the tension surface. Using a similar analysis to that used for the uncracked section Reference 1 developed equations for the neutral axis depth and equivalent steel I as follows

$$d_n^2 + \left[2A_s(N - k + 1 - \frac{E_s}{E_c}N) - 2t\right]d_n + \left[2A_s(\frac{E_s}{E_c}\sum_{i=1}^{N} d_i - \sum_{i=k}^{N} d_i) + t^2\right] = 0 \qquad (3.5)$$

and

$$I_c = A_s \sum_{i=1}^{N}(d_n - d_i)^2 + \frac{1}{3}\frac{E_c}{E_s}\left[(t - d_n)^3 - 3A_s\sum_{i=k}^{N}(d_n - d_i)^2\right] \qquad (3.6)$$

where the 'k^{th}' layer of reinforcement is immediately above the neutral axis. The introduction of 'k' is to allow for the area of concrete lost to the steel in the compression side of the section.

A computer solution can easily be written to find a value of

d_n satisfying equation 3.5 by an iterative procedure. A computer program for analytic solution of the quadratic equation was written for Reference 1, but it was found to be more complex.

For manual calculation a trial and error method may need to be adopted by solving equation 3.5 for a range of values of 'k'.

However, when there is a little reinforcement in the compression surface or when a less accurate solution is required it is sufficient to ignore the consequences of introducing 'k'. The equation for d_n will then become, from the original equations in the analysis in Reference 1.

$$d_n^2 - 2 \left(A_s \frac{E_s}{E_c} N + t \right) d_n + t^2 - 2A_s \frac{E_s}{E_c} \sum_{i=1}^{N} d_i = 0 \qquad (3.7)$$

The resultant value of d_n is then substituted into equation 3.6 to find I_c.

3.3.1 General Behaviour at Failure

There are two characteristic modes of failure exhibited by reinforced concrete in bending, namely those of the 'under-' and 'over-reinforced' sections. In the former yield of the steel in tension occurs first and in the latter the conrete fails compressively whilst the steel is still behaving elastically. In general the characteristics for the bending of a simple beam would be as shown below.

Moment   Deflection   Deflection
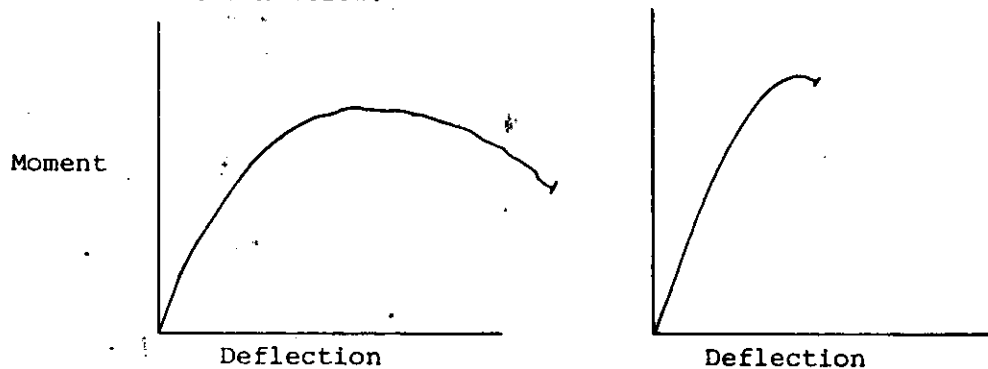
   (a)   Under-reinforced   (b)   Over-reinforced

Under-reinforcement allows relatively large deflections because of the steel's ability to experience strain up to a value of 0.10. For over-reinforcement the section fails by collapsing explosively with small deflections due to the limiting strain experienced by the concrete of 0.0035. Obviously the former quality is desirable for energy absorption. A 'balanced' section

can be idealised in which the steel reaches yield and the concrete in compression reaches its limiting strain at the same time. The balanced section is, in practice, variable because of any effects of membrane induced tensile forces, shear forces and the variability in the ultimate concrete strain. Thus, although it represents an economic combination of concrete and reinforcement, the balanced section is of little use in practice.

3.3.2 Conventional Limit State Analysis

A reinforced concrete section in ultimate bending does not behave plastically as can be seen from the diagrams above. The moment of resistance to bending is calculated on the stress profiles obtained when the concrete in the fibres at the surface of the compression face reach their limiting strain.

References 4 and 5, for example, consider this analysis in detail.

3.3.3 Concrete Stress Blocks

A variety of stress-strain 'blocks' are used for concrete in compression which have been developed for differing situations to find a satisfactory model for the compressive behaviour as defined by the tests available.

The stress blocks in use are quite varied according to simplicity for use in design, building regulations concerned and accuracy required.

It is important to realise that some stress blocks used in design contain a 'partial safety factor', (γ_m), which in 'CP 110' is 1.5. This must be accounted for when making the mathematical model for the failure section. The different stress blocks also use either the cube strength f_{cu} or the uniaxial compressive strength f_c'. They are related by

$$f_{cu} = 0.78f_c' \qquad (3.8)$$

Figure 1 shows a variety of stress blocks which are described below.

(a)   Hogenstead et Al.

This is the most accurate model which relates the area and the moment arm of the resultant force to the enclosing rectangle. The constants λ_2, λ_3 have been found experimentally and are presented empirically making use of this stress block tedious.

(b)   CP 110

This is a design curve from Reference 6. Adjustments to the tultimate stress have to be made accordingly. It is a simple parabolic curve up to a variable strain value defined by ε_{cu}, the ultimate stress being constant up to the limiting strain.

(c)   Witney

This is the most accurate rectangular stress block. The constant stress of $0.85f_c'$ has been derived to account for the shape limitation and moment arm and reduction in stress near to the edge due to shrinkage.

(d)   CEB

Reference 7 uses this stress block which is similar to the CP 110 one, but has the simplification of a fixed strain at the transition from the parabolic to the constant stress regions.

3.3.4   Comparison of Stress Blocks

The CEB stress block is used in the mathematical model for the failure section in section 3.3.5.

Witney and other stress blocks such as triangular, trapezoid and (b) and (c) from above were tried with the following observations.

For sections with very little reinforcement the neutral axis was so close to the compression face that the shape of the stress block becomes more critical in defining the location of the neutral axis and thus the resultant moment of resistance.

It was for this reason that the CEB stress block was chosen as the basis for the final model of the failure section because it possesses simple geometry with a good representation of the real shape. Any improvement in accuracy by using the Hogenstead stress block is not significant in this situation when applied to the failure of a panel.

3.3.5 Mathematical Model of the Failure Section

Cross Section   Stresses   Strain
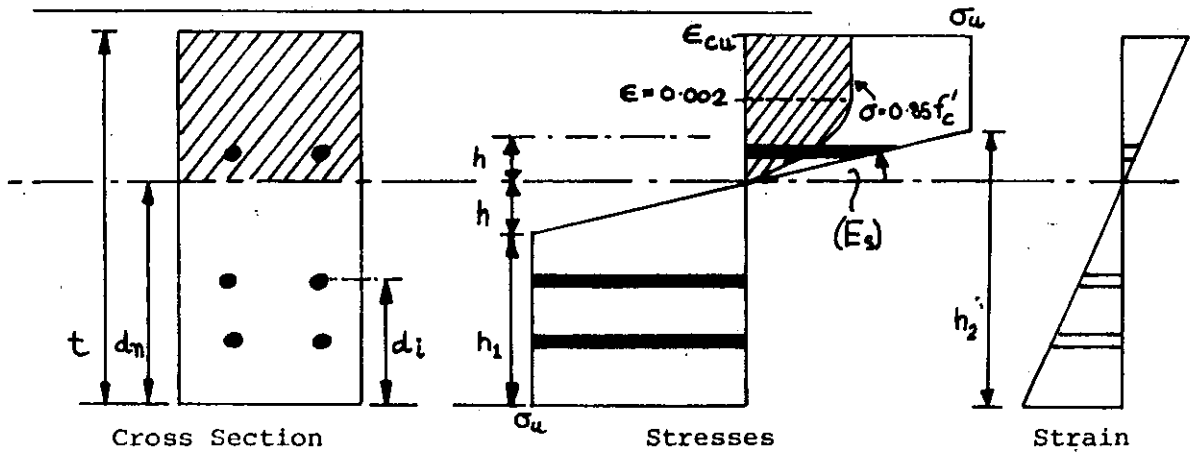
The final mathematical model for the failure section was made using the CEB stress block. The behaviour of the steel was modelled by a simplified version of the stress-strain diagram for single reinforcement strand tests from Figure 2. It was assumed that the the behaviour of the steel was similar in tension and compression.

Reference 1 includes the development of the expressions below from which the depth of the neutral axis and hence the moment of resistance to bending can be calculated.

Consider the horizontal forces on the components of the section, noting the simple mathematics of the parabolic stress block.

For the concrete, $\quad P_c = (t-d_n) \left[1 - \frac{1}{3} \left(\frac{0.002}{\varepsilon_{cu}} \right) \right] 0.85 \, f'_c$

For elastic steel, $\quad P_{SE} = \Sigma \, A_s \, \sigma_u \qquad\qquad 0 < d_i < h_1$
$$\left. \begin{array}{l} \\ \\ \end{array} \right\}$$
$\qquad\qquad\qquad\qquad - \Sigma \, A_s \, \sigma_u \qquad\qquad h_1 < d_i < t$

For plastic steel, $\quad P_{SP} = \Sigma \left(\frac{d_n - d_i}{h} \right) \sigma_u \, , \; h_1 < d_i < h_2$

$$\text{where } 2h = h_2 - h_1$$

The depth of the neutral axis d_n satisfies the equation for horizontal equilibrium,

$$P_c + P_{SE} + P_{SP} = 0 \tag{3.9}$$

Hence the moment of resistance of the steel and concrete components of the section are given by

$$M_c = (t-d_n)^2 \left[0.5 - \left(\frac{3}{10}\right) \times \frac{1}{3} \times \frac{0.002}{C_{cu}} \right] 0.85 f_c'$$

$$M_{SP} = \sum \left| (d_n - d_i) \right| \cdot A_s \sigma_u \qquad\qquad d_i < h_1, \; d_i > h_2$$

$$M_{SE} = \sum \frac{(d_n - d_i)^2}{h} \; \sigma_u \qquad\qquad h_1 < d_i < h_2$$

Then the total moment is given by

$$M_u = M_c + M_{SE} + M_{SP} \qquad\qquad\qquad (3.10)$$

4.0 THE APPLICATION OF CLASSICAL PLATE THEORY TO THE UNCRACKED PANEL

4.1 Isotropic Plate Theory - The Navier-Stokes Equation

The Navier-Stokes equation for the deflection of a simply supported square panel of side 'a' is derived in Appendix 2 as

$$w = \frac{16pa^4}{\pi^6 D} \sum_{n=1}^{\infty} \sum_{m=1}^{\infty} \frac{\sin\left(\frac{n\pi x}{a}\right) \sin\left(\frac{m\pi y}{a}\right)}{nm (n^2 + m^2)^2} = \frac{16pa^4}{\pi^6 D} k_i, \quad n,m \text{ odd} \qquad (4.1)$$

where the flexural rigidity used to compare isotropic to orthotropic plate theory is a mean of those of the two principal directions of the panel i.e.

$$D = \frac{1}{2} (D_x + D_y)$$

where $D_x = \frac{E I_x}{1-v^2}$

and 'I_x' is the second moment of area per unit width.

The values of the summation term k_i can be calculated by a simple computer program and have been tabulated for a series of co-ordinates in the panel, giving in particular from Figure 6.

(x/a : y/a)	k_i
1/2 : 1/2	0.2441
1/3 : 1/3	0.1873
1/2 : 1/4	0.1765
1/6 : 1/6	0.0663

4.2 Orthotropic Plate Theory

The equations governing orthotropic plate theory are included in Appendix 3. A similar expression to the Navier-Stokes solution for the deflection of the panel was obtained by another Fourier Series solution.

The solution leads to the following equation for the deflection of the panel, to illustrate the comparison with isotropic theory :

$$w = \frac{16a^4 p}{\pi^6 D_x} \sum_{n=1}^{\infty} \sum_{m=1}^{\infty} \frac{\sin\left(\frac{n\pi x}{a}\right) \sin\left(\frac{m\pi y}{a}\right)}{n m (n^2 + \lambda m^2)^2} = \frac{16a^4 p}{\pi^6 D_x} k_i', \quad n,m \text{ odd} \qquad (4.2)$$

where D_x is the flexural rigidity in one direction, taken as the smaller one.

and $\lambda = D_y/D_x$

Note that when $\lambda = 1$, the isotropic equation is returned where $D = D_x$.

Values of the summation factor k_i' have been plotted against λ and are shown in Figure 7.

4.3 Comparison Between Isotropic and Orthotropic Plate Theory

Mathematically, comparison between the theories can be established for a square panel as follows.

Consider the central point as the most sensitive to deflection. Isotropic and orthotropic theories respectively, give the deflections w_i and w_o where

From (4.1)

$$w_i = \frac{16a^4 p}{\pi^6 D} \sum_{n=1}^{\infty} \sum_{m=1}^{\infty} \frac{\sin\left(\frac{n\pi x}{a}\right) \sin\left(\frac{m\pi y}{a}\right)}{n\,m\,(n^2 + m^2)^2} = \frac{16a^4 p}{\pi^6 D} k_i$$

and (4.2)

$$w_o = \frac{16a^4 p}{\pi^6 D_x} \sum_{n=1}^{\infty} \sum_{m=1}^{\infty} \frac{\sin\left(\frac{n\pi x}{a}\right) \sin\left(\frac{m\pi y}{a}\right)}{n\,m\,(n^2 + \lambda m^2)^2} = \frac{16a^4 p}{\pi^6 D} k_i'$$

on division

$$\frac{w_i}{w_o} = \frac{k_i}{k_i'} \times \frac{D_x}{D} \tag{4.3}$$

where $D = \frac{D_x + D_y}{2} = (1 + \lambda)\frac{D_x}{2}$, since $D_y = \lambda D_x$ \qquad (4.4)

At the centre of the panel isotropic theory from Figure 3 gives $k_i = 0.2441$. Hence the value of $\frac{w_i}{w_o}$ can be calculated for various values of λ by reading k_i' from Figure 7 as follows

| λ	k_i'	$\left(\frac{w_i}{w_o}\right)$
1.0	0.2441	1.00
1.1	0.233	1.00
1.2	0.222	1.01
1.4	0.204	1.03
1.6	0.190	1.04
1.8	0.177	1.07
2.0	0.169	1.09

It is observed that for values of λ close to 1 the analysis gives similar central deflection. Consideration of the theoretical value of λ for a wide variation of wiremesh arrangements showed a range for λ of 1.0 - 1.2. Hence there was theoretically no value in applying orthotropic theory to square panels. Experiment showed that there was no significant difference in the deflections measured at similar points on orthogonal centrelines in the panels tested, thus supporting the theoretical conclusion.

4.4 Moment Fields in Simply Supported Panels

Various features of the panels in bending prompted an investigation of the moment fields in the panel. In particular, the formation of cracks which occured along the diagonals and in the central region of the panel. It was also observed that there was negative curvature along the diagonals towards the corners and this indicated the presence of negative moments in the panel.

The Navier-Stokes equation was used to calculate the moment field, expressing it in terms of the principal moments.

The diagram below illustrates the plane moment system in the Ont axes set.
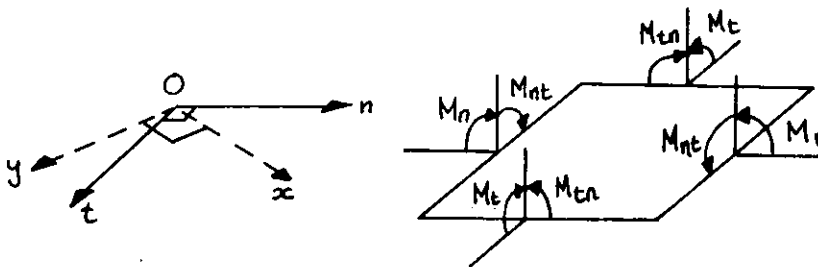
· M_n and M_t are principal moments in the plate if the 'twisting moment', $M_{nt} = 0$. $M_{nt} = -M_{tn}$.

These moments are directly related to the principal stresses since they arise from the integration of in-plane forces throughout the depth of the panel by equations A.2.4 and A.2.5.

Appendix 4 deals with the determination of the magnitude and direction of the principal moments from the Navier-Stokes equation.

A computer program was written to calculate the moment fields from the analysis using a value of Poisson's Ratio = 0.3.

The two principal moments were then plotted in contour form,from the values calculated on a grid on the panel,in Figure 8.

From Figure 8 the negative moments along the diagonals explained the negative curvature. The magnitudes of the principal moments are greatest across the diagonals and in the centre of the panel. This explained the features observed when the panel underwent transition.

4.5.0 Prediction of Panel Behaviour up to Initiation of Cracking (First Transition)

A series of 8 panels of identical dimensions, but differing mesh arrangement were accurately made as described in Reference 1. Details of panels are given in Appendix 5. From the measurements made in testing the panels the value of applying classical plate theory firstly to the prediction of deflections and secondly the first transition point was examined.

4.5.1 Prediction of Uncracked Panel Deflections

From the curves in Figures 9 to 16 showing the deflection of the panels with pressure it was observed that there was no initial linear elastic behaviour in most cases. Only the panels containing least reinforcement exhibited this linear behaviour and a well defined transition point. It was decided to use these curves for panels 1, 2, 3 to see if a consistent application of plate theory could be made.

An initial model of the uncracked section was made assuming that the concrete was continuous throughout the depth. Substituting this stiffness into the Navier-Stokes equation (4.1) in the form

$$\frac{w}{p} = \frac{16a^4}{\pi^6 D} \sum_{n=1}^{\infty} \sum_{m=1}^{\infty} \frac{\sin\left[\frac{n\pi x}{a}\right] \sin\left[\frac{m\pi a}{a}\right]}{n\,m\,(n^2 + m^2)^2} \qquad n,m \text{ odd} \qquad (4.5)$$

made the panels theoretically 40 - 50% too stiff, when compared with the measured $\left[\frac{w}{p}\right]$ slopes. Hence modification to the initial uncracked section was made.

One of the two alternatives to the initial model investigated used the assumption that Young's Modulus of concrete could be lower in tension than compression. An expression for the equivalent stiffness of the uncracked section where the Young's Modulus in tension and

compression held a constant fixed ratio was developed. In order
to get a good fit to these curves the required ratio was approximately
0.3 to 0.4. This value appeared to be too low and thus the model
was discounted.

The final model adopted the reasonably assumptions that the
panel contained initial cracking in the covering layer which was
effectively useless in tension. In view of the limited experimental
data obtained any assumptions made about the depth of initial cracking
in both of the orthogonal directions are of little significance.
An adequate stiffness for use in isotropic theory could be obtained
in two ways. Firstly, the I value way calculated in orthogonal
directions with an initial crack depth half a wire diameter below
the lowest layer as shown in (a) below and the mean value taken.
Alternatively, the panel could be considered cracked up to the lowest
level of reinforcement in either direction as in (b)

(a)   (b)
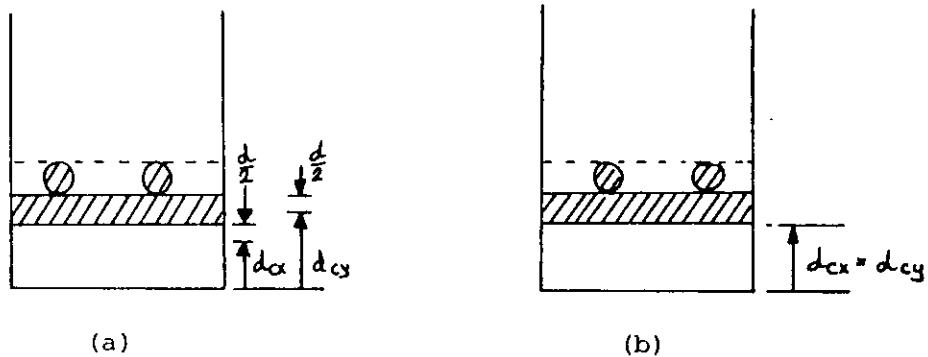
As mentioned above there was no significant difference between
the two methods, but in view of the fact that the stiffness of the
uncracked panel was dominated by the concrete and that the uncracked
phase of the panel deflection was limited in most cases anyway, it
is convenient to use the second method and consider the panel as
a solid panel of concrete with an ineffective surface layer in tension.

It was also observed that the shape of panels 1,2 and 3 as
defined by the deflections at other points on the surface followed
that given by the Navier-Stokes equation.

Finally, it was observed from the panels with most reinforcement
and little if any initial linear elastic behaviour that applying this
method did at least give a reasonable tangent to the slope at the origin.

4.5.2 Prediction of the First Transition Point

From the pressure-deflection curves for panels 1,2 and 3 a distinct transition point can be identified which corresponds to the initiation of cracking in the panel. An investigation was made in order to determine a criterion for this transition point.

The initiation of cracking will occur when the concrete can no longer stand the maximum local tensile stress.

The Navier-Stokes equation (4.1)

$$w = \frac{16pa^4}{\pi^6 D} \sum_{n=1}^{\infty} \sum_{m=1}^{\infty} \frac{\sin\left(\frac{n\pi x}{a}\right) \sin\left(\frac{m\pi y}{a}\right)}{n\, m\, (n^2 + m^2)^2} \qquad n,m \text{ odd} \qquad (4.6)$$

was used to calculate the local stresses in the panel. From equation (A.2.4), the equation for the stress at a distance Z from the neutral axis of the panel in the Ox direction is

$$\epsilon_{xx}(Z) = \frac{Z}{1-\nu^2} \left[\frac{\partial^2 w}{\partial x^2} + \nu \frac{\partial^2 w}{\partial y^2} \right]$$

$$= \frac{Z}{1-\nu^2} \left[\frac{\pi^2}{a^2} \right] \frac{16pa^4}{\pi^6 D} \sum_{n=1}^{\infty} \sum_{m=1}^{\infty} \frac{\sin\left(\frac{n\pi x}{a}\right) \sin\left(\frac{m\pi y}{a}\right)}{n\, m\, (n^2 + m^2)^2}$$

$$= \frac{Z}{1-\nu^2} \left[\frac{\pi^2}{a^2} \right] \frac{16pa^4}{\pi^6 D} k_2 \qquad (4.7)$$

Hence the stress is

$$\sigma_{xx}(Z) = E_c \, \epsilon_{xx}(Z) \qquad (4.8)$$

It follows from Figure 8 that the maximum principal moments and hence stresses occur in the corners of the panel. Calculations of the tensile stresses in the corners gave exceptionally high predicted values of stress. Because of this and doubt about the physical conditions at the corners it was decided to use the centre of the panel as the point of reference. Visual observation also showed that cracking appeared at the centre and along the diagonals of the panels simultaneously.

At the centre of the panel the principal stresses are equal and in the O_x and O_y directions and here equations 4.7 and 4.8 become,

with $k_2 = 0.2921$,

$$\sigma(Z) = Z \; \frac{16pa^2}{\pi^4 I_u} \; \frac{E_c}{E_s} \times 0.2921 \qquad (4.9)$$

by substituting for 'D'. The maximum principal tensile stress in the panel is obtained by substitution for Z as the distance from the neutral axis to the extreme depth of concrete. From section 4.5.1 it was found that the panel behaved as though it was cracked through the surface covering layer so the value of Z used was the distance from the neutral axis to the depth of the lowest layer of reinforcement.

It was decided to relate the maximum tensile stress calculated at the centre of the panel to the Modulus of Rupture, given in Appendix 1 as

$$f'_{ct} = 0.6225 \; \sqrt{f'_C} \qquad (4.10)$$

This gave values of $\dfrac{\sigma(Z)}{f'_{ct}}$ for each of panels 1, 2 and 3 as 2.50, 2.23 and 2.16 respectively. A mean value of

$$\frac{\sigma(Z)}{f'_{ct}} = 2.3 \qquad (4.11)$$

was taken as the criterion for locating the first transition point for these panels.

The most important observation to be made is the large amount by which the predicted stress exceeds the maximum empirical tensile stress of the concrete at the centre of the panel. There are many assumptions which have been made which can alter the relationships of the calculated stress and the Modulus of Rupture such as the working value of Young's Modulus used, and the value of Z taken. It is known that Young's Modulus for concrete in tension can vary from the compressive value. The Modulus of Rupture is an empirical value and thus subject to a degree of uncertainty and it is also known that well-reinforced concrete can sustain a significant increase in tensile stress.

Using the criterion of equation 4.11 the transition point was predicted for the remaining panels, 4 - 8. Even though no distinct transition point is present, the general observation was that transition appeared to occur earlier with an increasing amount of reinforcement. In fact, in the case of panel 8 with the most

reinforcement it appeared that transition could have been considered to occur at the origin.

Further discussion of first transition is included in section 5.2 with regard to the prediction of cracked panel deflection.

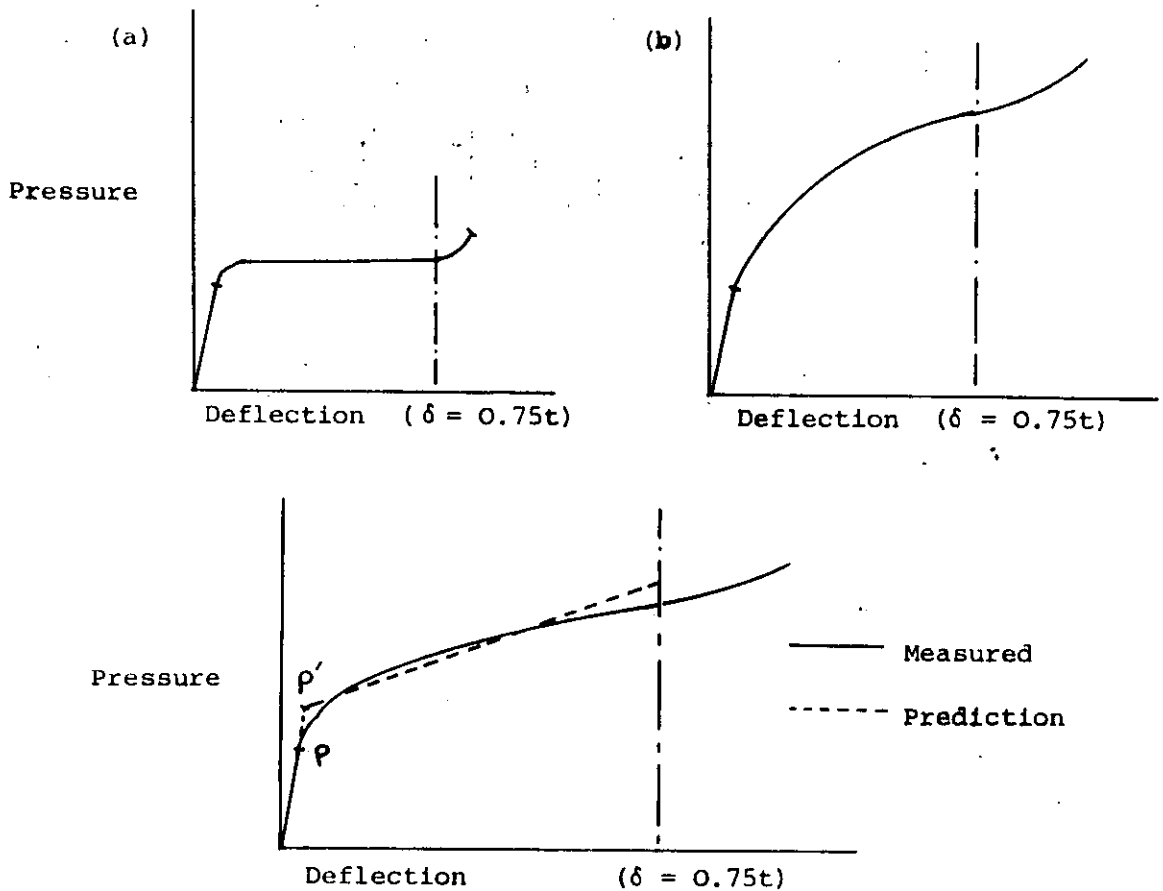## 5.0 EXTENSION OF CLASSICAL PLATE THEORY TO THE CRACKED PANELS

5.1 General Behaviour of A Cracked Panel

Central Deflection ($\delta = 0.75t$)
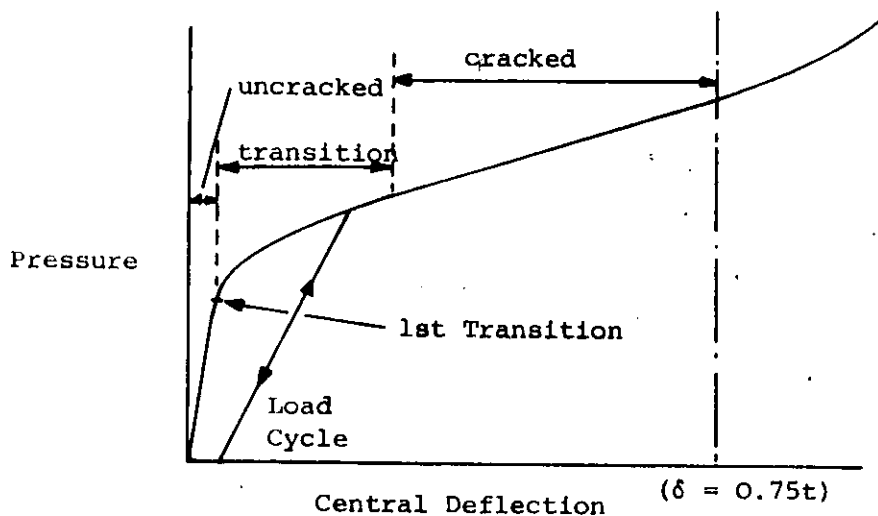
An idealised form of the pressure-deflection curve for a ferrocement panel is shown above. It features the initial linear elastic behaviour up to the first transition point where cracking begins. The next stage is of transition to a fully cracked panel. The panel effectively behaves elastically in both the uncracked and cracked phases. This does not however mean that the panel will return to zero deflection when unloaded from a point above the uncracked phase, but will have an initial 'set' as shown above by a typical load / unload cycle. This is explained because the panel changes it structure when it cracks. The panel now has many open discrete cracks, but it still behaves effectively elastically since no yielding has occurred in the reinforcement.

The duration of the transition stage depends on the amount of reinforcement in the panel. For instance the panel could reach transition and go straight to failure as shown in (a) below; or the transition period may be so extended that a fully cracked panel is not achieved before the interference of membrane action as in (b).

To extend classical plate theory to the cracked panel in the ideal case shown below, the first transition point, P, and the extent of the transition phase would be calculated in order to find an equivalent transition point, P', from which the prediction can be extended. However, because of the variation of behaviour in practice with reinforcement arrangement, the predictions were based on the first transition point only and observations made on this assumption.

(a)

Pressure

Deflection (δ = 0.75t)

(b)

Deflection (δ = 0.75t)

Pressure

ρ′

ρ

——— Measured

------ Prediction

Deflection (δ = 0.75t)

5.2 Fully Cracked Panel Predictions of Deflection

The pressure-deflection slope for the fully cracked panel was calculated using the flexural rigidity, as a mean of those of the O_x and O_y directions, given by the cracked section in the Navier-Stokes equation (4.5) This line was extended from the first transition point as calculated from Section 4.5.2 The predictions were drawn on Figures 9 to 16 from which the following observations were made.

For the identical panels 1 and 2, with one layer of reinforcement, it appeared that the panels transformed straight into a failure mode. In the case of panels 3, 4, 5 and 7, with 3 or 4 layers of reinforcement, the predictions formed a fairly good envelope to the behaviour. The two exceptional cases were panel 8 with most reinforcement and panel 6 with a diagonal reinforcement arrangement. The prediction for the cracked section of panel 8 gives deflections which are too small and in fact it would have been better to have considered the panel initially fully cracked. In the case of panel 6 with diagonal reinforcement the transition was delayed, possibly as a consequence of mesh orientation, but further experimental evidence is needed to qualify this observation.

In conclusion, it was observed that the effective position of first transition occurred earlier with increasing reinforcement content. Clearly more experimental data has to be obtained before this behaviour can be confidently predicted, perhaps with regard to reinforcement direction as indicated by panel 6. However, the gradient of the pressure deflection curve was well predicted where a cracked phase was present.

5.3 Partially Cracked Panel Solutions

(a) $D = $ Const.
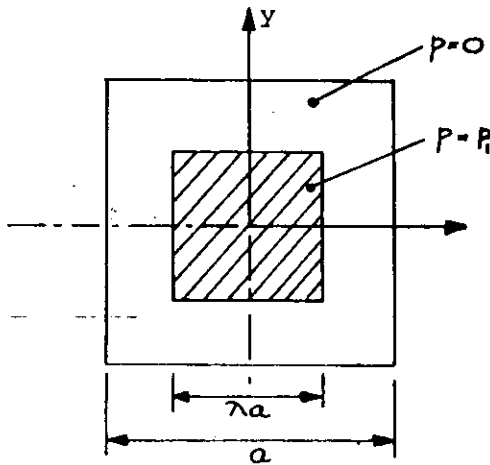
(b) $p = $ const.
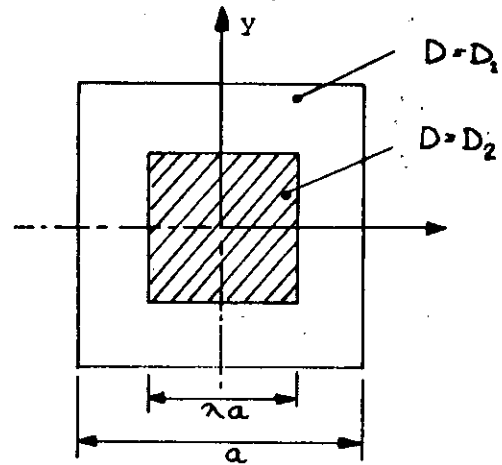
An investigation revealed two possible applications of classical plate theory as approximations to a panel with both cracked and uncracked regions. Observation indicated that the cracking occurred mainly in the central region and also along the diagonals. Two solutions were investigated.

Firstly a solution to a panel under a square central area of pressure was taken from Reference 8. Using the symbols in diagram (a) above the solution is

$$w = \frac{16a^4 p_1}{\pi^6 D} \sum_{n=1}^{\infty} \sum_{m=1}^{\infty} (-1)^{\frac{n+m}{2}} \frac{\sin\left(\frac{\lambda n\pi}{a}\right) \sin\left(\frac{\lambda m\pi}{a}\right) \sin\left(\frac{n\pi x}{a}\right) \sin\left(\frac{m\pi y}{a}\right)}{n\, m\, (n^2 + m^2)^2} \quad n, m \text{ odd}$$

$$(5.1)$$

The second approximation considered a panel of two stiffnesses as shown in diagram (b) above. This solution was developed in Reference 1 to give the following equation

$$w = \frac{16a^4 p}{\pi^6 \left[(1-\lambda^2)D_1 + \lambda^2 D_2\right]} \sum_{n=1}^{\infty} \sum_{m=1}^{\infty} \frac{\sin\left(\frac{n\pi x}{a}\right) \sin\left(\frac{m\pi y}{a}\right)}{n\, m\, (n^2 + m^2)^2} \qquad (5.2)$$

These methods were investigated in order to find an approximation to the $\left(\dfrac{w}{p}\right)$ slope of the panel in the cracked phase assuming it still contained both cracked and uncracked sections as defined by λ. However, since the cracked area, and hence λ, can vary with deflection and because an adequate prediction was more easily available by section 5.2 using the fully cracked approximation so further investigation into the application of this method was not continued.

5.4 The Initiation of Yielding

The existence of a second transition point at which the reinforcement begins to yield was investigated as follows.

It was assumed that the panel was completely cracked and the centre of the panel was taken as the location of maximum principal stresses. The calculation of this transition point was based on the overall deflection of the panel and not the pressure, since the strains in a panel are a geometric property depending on panel deflection. If the prediction had been based on pressure, then the location of the first transition point would have been of importance.

From the Navier-Stokes equation (4.1)

$$w = \left(\frac{16pa^4}{\pi^6 D}\right) k_1 \tag{5.3}$$

an expression for strain was obtained as equation (4.7)

$$\varepsilon = \frac{z}{1-\nu^2} \left(\frac{16pa^2}{\pi^6 D}\right) \frac{\pi^2}{a^2} k_2 \tag{5.4}$$

Hence, on division, where at the centre $k_1 = 0.2441$, $k_2 = 0.2921$

$$\varepsilon = \frac{0.2921}{0.2441} \frac{\pi^2}{a^2} \frac{z}{1-\nu^2} w \tag{5.5}$$

A yield strain of $\varepsilon = 0.004$ was taken from Figure 2 and the value of w thus calculated for each panel and drawn on Figures 9 to 16.

It was observed that there was no significant change of slope to give evidence of the transition. Note that the calculated values are close to deflection at which membrane action becomes significant. The spread of yielding in the panel will develop

over a wider range of panel deflection than the development of cracking. This is because the yield strain of steel is much higher than that of concrete at cracking. These reasons explain why a second transition point is not clearly visible.

6.0 ULTIMATE LOAD SOLUTIONS

### 6.1 Panel Failure Modes and Prediction of Failure Loads

Ultimate load theory relies on the definition of a mode of failure at which the panel collapses with a prescribed hinge pattern. The ultimate load solution usually considers the pattern which requires the least pressure for collapse by the hinge mechanism.

It was found from the panel tests that two modes of failure were observed. In the case of the panels with 1 or 2 layers of reinforcement only, cracks were observed along the diagonals as shown below as the 1st mode of failure. The second mode of failure was obeyed by the other panels and is also shown.
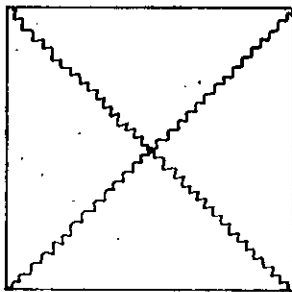
(a) Mode 1   (b) Mode 2
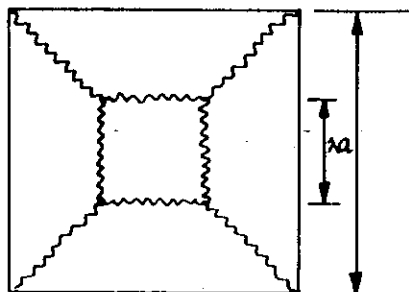
The theory used for calculating the relationship of failure pressure and hinge moment of resistance per unit width for both modes was considered in Reference 1. Although the two modes could be considered separately, the first is the limiting case of the second with $\lambda = 0$.

From Reference 1

Mode 2 : $M_p = \dfrac{pa^2}{24} (1-\lambda^3)$ or $p = \dfrac{24M_p}{(1-\lambda^3)a^2}$ $\qquad$ (6.1)

thus with $\lambda = 0$,

Mode 1 : $M_p = \dfrac{pa^2}{24}$ or $p = \dfrac{24M_p}{a^2}$ $\qquad$ (6.2)

The moment of resistance is calculated from the failure section as considered in Section 3.3.

In order to predict the failure pressure for Mode 2 the value of λ must be known. It was observed that the value was not constant during failure and so it was decided to use the value calculated

from measurements made at collapse. The failure pressures so
calculated are indicated on the Figures 9 to 16.

It was observed that the predictions were all very low.
The most likely reason was the presence of membrane forces at very
large deflections. The effect of the orientation of the reinforcement
on the hinge moment of resistance was considered in Section 6.2. It
was also noticed that excessive hinge movements allowed the edges of
the panels to be restrained. This was only significant in the case
of panel 7 where the failure pressure could not be safely reached.
It was taken up to 16 N/cm^2 whereas comparable panels reached 9 - 10
N/cm^2.

6.2 The Effect of Mesh Orientation on the Failure Moments

The orientation of the wiremesh can affect the failure
moment if kinking of the wiremesh develops across cracks in
the hinge as shown below
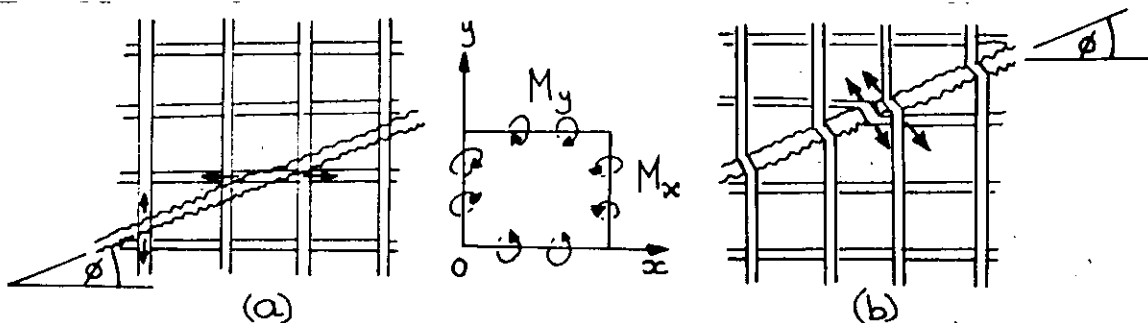
Consider the moment along a hinge at an angle ϕ to the O_x
direction. Suppose that M_x and M_y are principal moments so that
$M_{xy} = 0$. Then from equation A.4.1.

$$M_n = M_x \cos^2 \phi + M_y \sin^2 \phi \tag{6.3}$$

Thus for case (a) above, where there is no kinking of wiremesh,
the failure moment for an isotropic panel with component failure
moments $M_x = M_y$ is

$$M_u = M_x (\sin^2 \phi + \cos^2 \phi) = M_x \tag{6.4}$$

i.e. it is independent of direction.

This is an upper-bound solution. A 'lower-bound' solution
exists where the effect of the twisting moment is included in (6.3).

It is found, however, that twisting moments have very little effect on failure moments.

Diagram (b) above shows the effect of reinforcement kinking across a wide crack. Resolving moment vectors along a unit length of the hinge now gives

$$M_n = M_x \cos \phi + M_y \sin \phi \tag{6.5}$$

The maximum effect for an isotropic panel occurs when $\phi = 45^{\circ}$ when $M_x = M_y$ so that

$$M_u = 2 \frac{M_x}{\sqrt{2}} = \sqrt{2} M_x \tag{6.6}$$

Thus the kinking of the mesh in a wide crack could give up to 40% more moment of resistance. This is clearly restricted since complete kinking is unlikely to occur because the concrete would crumble first.

In order to investigate this effect panel number 6 was arranged with the reinforcement parallel to the diagonals. It was to be compared with panels 4 and 5 which were similar but with reinforcement parallel to the edges. However, since these panels failed in Mode 2, thus with reinforcement both parallel and diagonal to the hinge elements, and number 6 in Mode 1, no significance could be attached to the result. In fact all three panels failed at approximately 10.0 N/cm^2.

In the case of panels 1 and 8 each with only one layer of reinforcement the first mode of failure was observed. Thus with the reinforcement placed parallel to the edges the wiremesh strands were at the diagonal to the hinges. Kinking of the strands was actually visible. However, even increasing the moment of resistance by the factor of $\sqrt{2}$ as given by Equation 6.3 the prediction of the failure is still too low as shown on Figures 9 and 10.

6.3 Prediction of Beam Failure Modes

Reference 10 gives experimental data on the results of testing ferrocement beams under a constant bending moment. Of particular interest here is the prediction of the failure load of the beams. A re-analysis of the predictions made in Reference 10 using the failure section of section 3.3.5 gives better agreement. Typical load-deflection diagrams with predictions of failure loads are shown in

Figures 17 and 18.

It was observed that the failure section can be used to
give a good approximation to the ultimate load for simple bending.
This contrasts with the poorer predictions made for the panels in
section 6.2 which are most likely attributed to the causes listed
there. However, the predictions made for the beams were all
consistently low leaving uncertainty as to whether this was due
to any limitations in experimental technique or theoretical
considerations.

7.0 CONCLUSIONS

From the experimental and theoretical work in this report the following observations have been made.

1. By increasing the reinforcement content, the general properties of the panel improve such that the maximum load and deflection are increased. With more reinforcement, cracking in the panels was dispersed over larger areas. The stiffness of the panels is mostly dependent upon the outer layers and does not differ significantly in the principal directions of the reinforcement.

2. It was found both theoretically and experimentally that the application of isotropic plate theory was quite sufficient for square panels and would certainly be so for a low aspect ratio with this type of arrangement. Orthotropic plate theory need only be considered when there are large differences in the directional properties of the material such as when longitudinal steel rods are included in the construction.

3. The use of isotropic plate theory to predict the deflections of the uncracked panel require that the panels be considered to have an ineffective surface layer in the tension surface. The stiffness of the panels is calculated by assuming that the 'uncracked' section has an initial crack in the surface layer up to the lowest level of the reinforcement.

4. From tests of panels with 1 or 2 reinforcement layers, a transition point was evident. The following criterion exists at this point

$$\sigma = 2.3 \ f'_{ct}$$

where σ is the maximum fibre stress in the concrete at the centre of the panel and at the depth of the lowest layer of reinforcement. f'_{ct} is the 'Modulus of Rupture' from Appendix 1;

$$f'_{ct} = 0.6225 \ \sqrt{f_{ct}}$$

Applying this criterion to the initiation of cracking in the other panels indicated that transition appeared to occur earlier with increasing reinforcement content. It was also observed that the orientation of the reinforcement affected transition.

Some research has been carried out, Reference 12, to investigate cracking which is important as a limit on service to maintain water-tightness and so prevent reinforcement corrosion. The general

conclusion of these investigations has been that the transition
stress increases with reinforcement content which contradicts the
observations made here. This reference also shows that the stress
in the concrete at transition varies between 0.5 - 4.0 f'_{ct} , depending
on the varying assumptions made. This confirms the accepted increase
in tensile strength of concrete due to the presence of reinforcement.

5. The mathematical model of the cracked section can be used
to reasonably predict the slope of the pressure-deflection curve in
the cracked phase. The accuracy of the prediction of cracked panel
deflections by extending this slope from the first transition point
depends on the location of the transition point as indicated in (4).
In particular, for panel 8 with most reinforcement sufficient
accuracy could be obtained by drawing the cracked phase from the
origin of the pressure-deflection diagram.

6. The use of limit state theory in the prediction of failure
loads for simple beams is good. However, predictions for panel
failure were too high because of the complications introduced by
membrane forces etc.

        This report shows the value of applying classical plate theory
in a simple way to ferrocement panels. The initial tests have
shown this as a promising method of predicting panel deflection.
However, further information is required in order to calculate
the effective first transition point to extend the prediction into
the cracked phase. Further investigation should also be carried
out with regard to the prediction of panel failure loads although
the simple application of limit state theory provided a consistently
safe estimate in these tests reported.

8.0 RECOMMENDATIONS

In order to construct a complete picture of the behaviour of ferrocement to large deflections more experimental data must be obtained on the initiation of cracking with regard to reinforcement arrangement. From the work done it is clear that reinforcement content is significant and so also is reinforcement orientation. Other factors will also affect transition, for example, the reinforcement type and the thickness of the covering layer over the reinforcement. Such experiments may well give better results by using wide beams or panels in cylindrical bending thereby eliminating the complication of double curvature with fully supported panels of low aspect ratio. Attention is drawn to various articles concerning cracking of ferrocement such as References 12 and 13.

Finally more information is required to assess the problems involved in the prediction of failure loadings of panels using limit state analysis, including the effects of mesh orientation.

LIST OF REFERENCES

1. "AN INVESTIGATION INTO THE APPLICATION OF CLASSICAL PLATE
    THEORIES TO THE BEHAVIOUR OF A FERROCEMENT PANEL".
    D. R. Prentice, B.Sc. Hons. Report, 1979, Southampton
    University.

2. "THEORY AND ANALYSIS OF PLATES - CLASSICAL AND NUMERICAL
    METHODS" Rudolf Szilard. Prentice-Hall Publications. Civil
    and Mechanical Engineering series.

3. "CRACKING ANALYSIS OF REINFORCED CONCRETE PLATES - ELASTIC,
    POST-ELASTIC ANALYSES OF A TENSION WEAK MATERIAL".
    Wanchoo, M. K. and May, G. W. A.S.C.E. Journal -
    Structural Division, VlOl, nl, January 1975.

4. "FUNDAMENTALS OF REINFORCED CONCRETE". John R. Cernica,
    Addison-Wesley 1964 Publishing Co. Ltd.

5. "LIMIT-STATE DESIGN OF REINFORCED CONCRETE". Derek Beckett,
    Surrey University Press.

6. "CODE OF PRACTICE FOR THE USE OF CONCRETE : 1972"
    British Standards Institute CPllO.

7. "INTERNATIONAL RECOMMENDATIONS FOR THE DESIGN AND CONSTRUCTION
    OF CONCRETE STRUCTURES". Comité European du Breton, English
    Edition: Cement and Concrete Association, June 1972.

8. "THEORY OF PLATES AND SHELLS" S. P. Timoshento and S. Woinowski-
    Kreiger. McGraw Hill Book Co. Inc.

9. "SHORT TIME DEFLECTIONS OF RECTANGULAR, RESTRAINED, REINFORCED
    CONCRETE SLABS". P. Desayi and K. U. Muthu. Proceedings
    of the Institute of Civil Engineers Part 2, June 1979.

10. "AN INVESTIGATION INTO THE BEHAVIOUR OF FERROCEMENT BEAMS
    SUBJECT TO PURE BENDING" P. J. Denton, B.Sc. Hon. Report
    1979, Southampton University.

11. "METHODS OF TESTING CONCRETE". British Standards Institute
    B.S.1881.

12. "F.A.O. INVESTIGATES FERROCEMENT - LABORATORY ANALYSIS,
    CONSTRUCTION METHODS, SERVICE EXPERIENCE" John Fyson
    Published by Fishing News (Books) Ltd., 1973.

13. "FERROCEMENT - A SURVEY" Dr. Ing Walkus and T. G. Kowalski
    Concrete : The Journal of the Concrete Society, Feb. 1971.

A.1.O. MATERIAL PROPERTIES

A.1.1 The Properties of Concrete

Structure

Concrete consists of a mixture of aggregate and cement. The aggregate consists of fine crystalline solids of rock and is bound together by the cement which is formed of colloidal lumps of solids. Many references to the many types of cements and aggregates are easily available such as reference 4.

The strength and the properties of the concrete depend on many factors from the earliest stages of mixing and proportioning to curing etc.

Compressive Strength

This is the most important property of concrete. Simple crushing tests indicate a typical strength of 40 N/mm^2. It is from this figure that the Grade number is taken, as Grade 40, 50 etc. The easiest test to perform is the cube test. Small cubes of the mix are made typically 5 or 10 cm wide and crushed to find the cube strength f_{cu}.
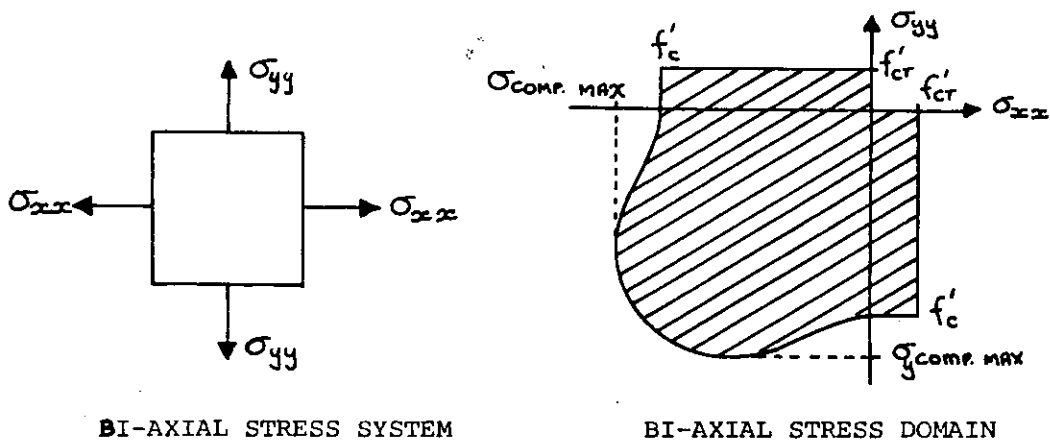
The direct uni-axial compressive stress f'_c is obtained from the crushing of cylindrical test-pieces where there are no weakening shape effects. The cube strength and direct uni-axial compressive strength are related by

$$f_{cu} = 0.78 \ f'_c$$

for ordinary strength concrete.

The maximum compressive strength of concrete is variable under a bi-axial state of stress. Consider the element in diagram (a) below, then the compressive strength in one principal direction can be related to the applied stress in the orthogonal direction. This is shown by diagram (b)

BI-AXIAL STRESS SYSTEM   BI-AXIAL STRESS DOMAIN

There is typically an increase of up to 20% over the uni-axial compressive stress.

Compressive strength increases with curing time as a consequence of the diffusion of the water into the colloids of cement in the curing process.

The variation of strength with time is shown in Figure 3. Normally a 28 day curing strength at 20°C is used since the rate of change of strength with time is then low, though 3 and 7 day strengths are useful in the short term.

Tensile Strength

Compared with the compressive strength the tensile strength is very low. It is about 7 - 10% of the compressive strength in uni-axial tension. The tensile stress as found from concrete beam tests is called the 'Modulus of Rupture'. It has accepted empirical forms such as the following from Reference 9

$$f'_{ct} = 0.6225 \sqrt{f'_c}$$

Simple tensile tests are difficult to perform and are usually done as a combination experiment by jacketing the test piece in a metal sheath.
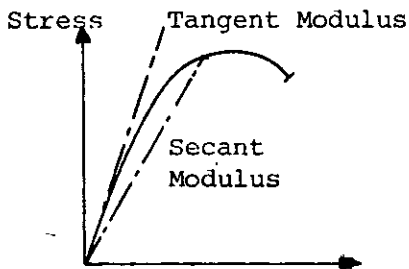
Although it is small the tensile strength helps to resist cracking due to thermal shrinkage and horizontal shear effects in beams. The tensile strength of a reinforced concrete can be significantly higher than when unreinforced.

Shear Strength

Although it is not referred to directly in this report the shear strength is worthy of note since it is low. Shear strength is dependent to a large extent on the interlocking of the aggregate grains. Thus a better aggregate increases the shear strength. In general it is about 0.15 - 0.25 of the compressive strength.

Modulus of Elasticity

Concrete does not have an initially linear stress-strain relationship as is diagrammatically illustrated below. Thus an initial tangent modulus or secant moduli for various working stresses can be defined. There is also the complication of creep effects and a dynamic modulus can also be obtained. In tension the elastic modulus can also vary because of the presence of initial cracks due to drying and other effects, but no specific reference could be found as to these effects. A typical experimental stress-strain curve is drawn on Figure 5.

Creep

Although this was possibly of no importance here due to the short duration of the tests, the effects of creep are worth mentioning. Creep is an effect of squeezing the water content out of the colloidal solids of the cement under pressure. It can be measured in a very slow compression test, but it is most important in long term applications of concrete, i.e. months or years.

Poisson's Ratio

Again this property is dependent to a small extent on the other variables in concrete, but in general it is assumed to take the value of $\nu = 0.20 - 0.25$ for normal weight concrete.

Coefficient of Coverage

The coefficient of coverage is a measure of the dispersion of steel in a reinforced concrete component. It is defined as

$$K_x = \frac{\text{surface area of steel in contact cement}}{\text{volume of concrete}}$$

A value of K_x greater than 0.1mm^{-1} has been suggested to delineate ferrocement from ordinary reinforced concrete.

Also useful in describing the reinforcement content is the ratio of weights of steel to concrete. A typical range of values for ferrocement construction is 10 - 25%

A.1.2 Testing of Concrete

In order to determine the characteristic properties of the concrete in a ferrocement structure test pieces in the form of cubes and prisms are made from the original mix and cured with the parent structure. Various methods of determining the properties are available and these are now reviewed.

The compressive strength is found from cube tests. Cube testing is done in a hydraulic press in accordance with the strain rate and other conditions specified by B.S. 1881, Reference 11. It requires that the cubes are tested damp on removal from the curing tanks so that cracking on a microscopic level does not occur in drying out.

In order to determine Young's Modulus there are three simple approaches available. Firstly, there are many empirical diagrams such as Figure 4 relating parameters such as density and cube strength to Young's Modulus. Ultrasonic testing is the second method which uses sonic probes attached to prisms or cubes to measure the speed of sound in concrete, c. Then Young's Modulus can be calculated, essentially from

$$ c = \sqrt{\frac{E_c}{\rho}} $$

but with standard corrections for shape effects and Poisson's Ratio. This is a convenient on-site test method which is more reliable on large test pieces. Finally, direct measurement by strain gaugeing prisms and loading, by an Instron machine for example, inherently forms the most accurate method of taking measurements of stress and strain to obtain Young's Modulus. It must be noted that care has to be taken to attach the strain gauge well to the porous surface of the concrete. Direct measurements by an Instron machine are difficult because concrete will only experience a very small elastic strain of 0.0015 which can not easily be accurately detected unless long and relatively thin test pieces are used.

From the investigation carried out in Reference 1 it was found from strain gauge experiments that the empirical methods

were reliable and that ultrasonic testing on small test pieces produced unreliable results. Thus it was concluded that empirical methods are quite sufficient.

A.1.3 Testing of Wiremesh

To assess the characteristics of the wiremesh reinforcement tensile tests must be carried out. The simplest method available is that of single wire tests by an Instron machine although it is likely that testing a wide strip of reinforcement mesh will give a better overall assessment of behaviour.

Typical wiremesh is made of poor grade steel and can have a variety of surface finishes. The reinforcement used in the panels tested was galvanised and in order to calculate stress loadings the calculations were done on the area of the steel beneath the thin, weak galvanised coating. Removal of galvanising by acid attack or scraping allowed accurate measurement of the wire diameter to be made.

Consequently it was found that the wire had a low value of Young's Modulus of 145 GN/m^2 compared with the universally accepted range of 200 - 210 GN/m^2. It also achieved high ultimate strains indicating the poor quality of the material. The presence of the weld spots on the welded square mesh was also considered to be a contributory factor.

A stress-strain diagram is shown on Figure 2 and further details included in Appendix 5.

A.2.0 GENERAL PLATE EQUATIONS

A.2.1 The Biharmonic Equation
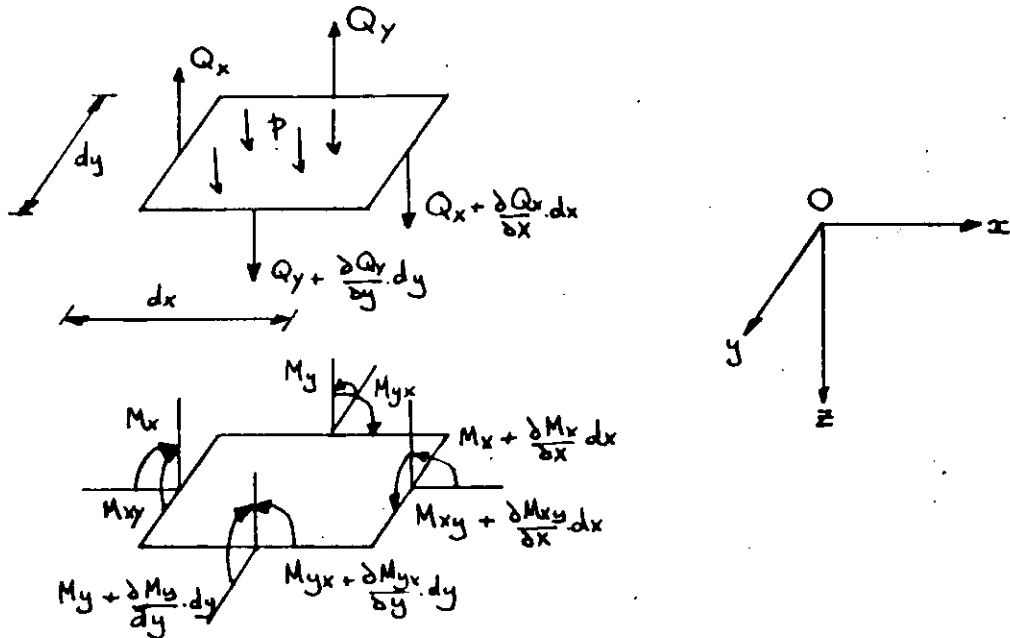
Consider a plate element under a shear force and bending moment system as illustrated above in the Oxy plane.

There are no in-plane membrane forces.

The panel is subject to a constant pressure p.

Let Q_x , Q_y = shear forces / unit length

M_x , M_y , M_{xy} = bending moments / unit length.

Then, for shear force equilibrium

$$\frac{\partial Q_x}{\partial x} dx\, dy + \frac{\partial Q_y}{\partial y} dy\, dx + p dx\, dy = 0$$

(A.2.1)

i.e. $\quad \frac{\partial Q_x}{\partial x} + \frac{\partial Q_y}{\partial y} + p = 0$

and for moment equilibrium

$$\frac{\partial M_y}{\partial y} dx\, dy - \frac{\partial M_{xy}}{\partial} d\quad d \quad - Q_y\, dy\, dx = 0$$
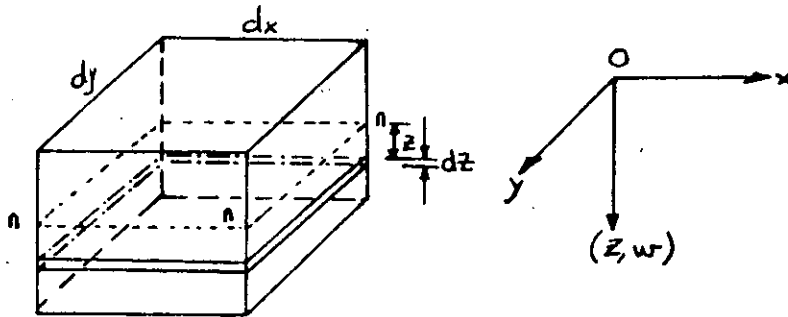
i.e. $\dfrac{\partial M_y}{\partial y} - \dfrac{\partial M_{xy}}{\partial x} - Q_y = 0$

similarly $\dfrac{\partial M_x}{\partial x} + \dfrac{\partial M_{xy}}{\partial y} - Q_x = 0$

$\hspace{10cm}$ (A.2.2)

Note that the complementary twisting moments $M_{xy} = - M_{yx}$.

From equations A.2.2 and A.2.1 the shear force terms can be eliminated to give

$$\frac{\partial^2 M_x}{\partial x^2} + \frac{\partial^2 M_y}{\partial y^2} - 2\frac{\partial^2 M_{xy}}{\partial x\,\partial y} = -p$$

$\hspace{10cm}$ (A.2.3)

The Relationship Between Bending Moment and Curvature

Consider an elemental section of the plate dxdy as a slice of thickness dz in the Oxy plane at a distance z from the neutral axis.

Let the curvature be defined by single curvature components about the Ox and Oy axes respectively.

Strain in the x-direction due to curvature about Oy only is

$$\varepsilon_x = z\frac{\partial^2 w}{\partial x^2}$$

From the elastic equations

$$\varepsilon_x = \frac{\sigma_x}{E} - \nu\frac{\sigma_y}{E}$$

$$\varepsilon_y = \frac{\sigma_y}{E} - \nu\frac{\sigma_x}{E} = 0$$

Hence for single curvature only

$$\varepsilon_x = (1-\nu^2) \frac{\sigma_x}{E}$$

i.e. $$\sigma_x = \frac{E}{(1-\nu^2)} \varepsilon_x$$

Superimposing the effect of curvature in both directions and substituting for the strain components

$$\sigma_x = \frac{E}{1-\nu^2} \varepsilon_x + \nu \frac{E}{1-\nu^2} \varepsilon_y$$

i.e. $$\sigma_x = \frac{EZ}{1-\nu^2} \left[\frac{\partial^2 w}{\partial x^2} + \nu \frac{\partial^2 w}{\partial y^2} \right]$$

and $$\sigma_y = \frac{EZ}{1-\nu^2} \left[\frac{\partial^2 w}{\partial y^2} + \nu \frac{\partial^2 w}{\partial x^2} \right]$$

(A.2.4)

Integration through the depth of the panel gives the moments per unit width

$$M_x = \int_{Z_1}^{Z_2} x \, Z \, dZ$$

$$\therefore \quad M_x = - D \left[\frac{\partial^2 w}{\partial x^2} + \nu \frac{\partial^2 w}{\partial y^2} \right]$$

and $$M_y = - D \left[\frac{\partial^2 w}{\partial y^2} + \nu \frac{\partial^2 w}{\partial x^2} \right]$$

(A.2.5)

where D is the 'flexural rigidity' of the panel given by

$$D = \frac{EI}{(1-\nu^2)}$$

where 'I' is the second moment of area of the panel per unit width about the neutral axis.

Now consider the shear in the elemental slice as taken above. Suppose that the element is subject to displacements u and v in the Oxy plane as shown below. Let displacement of the panel in the z-direction be w. For small deflections the shear in the Oxz and Oyz directions is negligible.
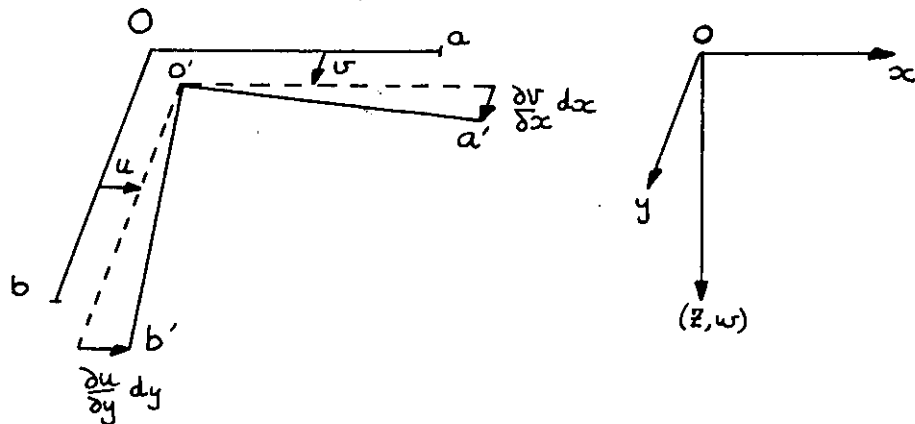
The shear stresses are given by

$$\gamma_{xy} = \left(\frac{\partial u}{\partial y} + \frac{\partial v}{\partial x}\right)$$

$$\gamma_{yz} = \left(\frac{\partial v}{\partial z} + \frac{\partial w}{\partial y}\right) = 0 \qquad \text{Hence} \qquad u = - z \frac{\partial w}{\partial x} + C$$

$$\gamma_{zx} = \left(\frac{\partial w}{\partial x} + \frac{\partial u}{\partial z}\right) = 0 \qquad \text{Hence} \qquad v = - z \frac{\partial w}{\partial y} + D$$

Since $u = 0$ when $w = 0$, then $C = D = 0$

Hence the shear stress is given by

$$\tau_{xy} = G \, \gamma_{xy} = 2G \frac{\partial^2 w}{\partial x^2}$$

Integration leads to the twisting moment, substituting $G = \dfrac{E}{2(1+\nu)}$

$$M_{xy} = \int_{z_1}^{z_2} \tau_{xy} \, z \, dz$$

$$M_{xy} = D(1-\nu) \frac{\partial^2 w}{\partial x \partial y}$$

(A.2.6)

Substitution for M_x, M_y, M_{xy} in A.2.3 leads to the Biharmonic equation

$$\frac{\partial^4 w}{\partial x^4} + 2 \frac{\partial^4 w}{\partial x^2 \partial y^2} + \frac{\partial^4 w}{\partial y^4} = - \frac{q}{D}$$

(A.2.7)

OR $\qquad (\nabla^4 w) = -\dfrac{q}{D}$ $\qquad\qquad\qquad$ (A.2.8)

A.2.2 Strain Energy in a Panel in Bending

The general expression for the total strain energy in a plate is

$$U = \int_v \left[\frac{\sigma_x^2}{2E} + \frac{\sigma_y^2}{2E} + \frac{\sigma_z^2}{2E} + \frac{\tau_{xy}^2}{2G} + \frac{\tau_{yz}^2}{2G} + \frac{\tau_{zx}^2}{2G} \right] \, dv \qquad\qquad (A.2.9)$$

Now, for small deflections it can be assumed that compared with σ_{xx}, σ_{yy};

$$\sigma_{zz} = \tau_{yz} = \tau_{zx} = 0$$

Thus

$$U = \int_v \left[\frac{\sigma_x^2}{2E} + \frac{\sigma_y^2}{2E} + \frac{\tau_{xy}^2}{2G} \right] \, dv$$

Substituting for σ_x, σ_y, τ_{xy} by equations (A.2.4) then

$$U = \frac{E}{2} \iiint_{xyz} z^2 \left\{ \frac{1}{(1-\nu^2)} \left[\left(\frac{\partial^2 w}{\partial x^2} + \nu \frac{\partial^2 w}{\partial y^2} \right)^2 + \left(\frac{\partial^2 w}{\partial y^2} + \nu \frac{\partial^2 w}{\partial x^2} \right)^2 \right] \right.$$

$$\left. + \frac{(1-\nu)}{(1-\nu^2)} \left(\frac{\partial^2 w}{\partial x \partial y} \right)^2 \right\} \, dz \, dy \, dx$$

$$= \frac{E}{2} \iiint_{xyz} z^2 \left\{ \left[\frac{\partial^2 w}{\partial x^2} + \frac{\partial^2 w}{\partial y^2} \right]^2 + 2(1-\nu) \left[\frac{\partial^2 w}{\partial x^2} \frac{\partial^2 w}{\partial y^2} - \left(\frac{\partial^2 w}{\partial x \partial y} \right)^2 \right] \right\} \, dz \, dy \, dx$$

$$\text{OR} \quad U = \frac{D}{2} \iint_{xy} \left[\frac{\partial^2 w}{\partial x^2} \quad \frac{\partial^2 w}{\partial y^2} \right]^2 \, dy dx + D(1-\nu) \iint \left[\frac{\partial^2 w}{\partial x^2} \frac{\partial^2 w}{\partial y^2} \quad \left(\frac{\partial^2 w}{\partial x \partial y} \right)^2 \right] \, dy \, dx$$

$$\qquad\qquad\qquad\qquad\qquad\qquad\qquad\qquad\qquad\qquad (A.2.10)$$

where $\quad D = \dfrac{EI}{1-\nu^2}$

It can be shown final integral term disappears for plates with no edge strain. Thus for a simply supported panel the strain energy is given by

$$U = \frac{D}{2} \iint_{xy} \left[\frac{\partial^2 w}{\partial x^2} \quad \frac{\partial^2 w}{\partial y^2} \right]^2 dx\, dy \qquad (A.2.11)$$

A.2.3 The Navier-Stokes Equation

A solution to equation (A.2.7) is developed as follows for a square panel of side a. Let the form of the deflection be

$$w = \sum_{n=1}^{\infty} \sum_{m=1}^{\infty} A_{mn} \sin\left(\frac{n\pi x}{a}\right) \sin\left(\frac{m\pi y}{a}\right) \qquad (A.2.12)$$

Then the strain energy in the panel is given by (A.2.11) as

$$U = \frac{D}{2} \int_A \left(\frac{\partial^2 w}{\partial x^2} + \frac{\partial^2 w}{\partial y^2} \right)^2 dA$$

$$= \frac{D}{2} \sum_{n=1}^{\infty} \sum_{m=1}^{\infty} \left(\frac{n^2\pi^2}{a^2} + \frac{m^2\pi^2}{a^2} \right)^2 A_{mn}^2 \int_{x=0}^{a} \int_{y=0}^{a} \sin^2\left(\frac{n\pi x}{a}\right) \sin^2\left(\frac{m\pi y}{a}\right) dy\,dx$$

Now, $\quad \int_{x=0}^{a} \sin^2\left(\frac{n\pi x}{a}\right) dx = \frac{a}{2}$

$$\therefore U = \frac{D}{8} \frac{\pi^4}{a^2} \sum_{n=1}^{\infty} \sum_{m=1}^{\infty} (n^2 + m^2)^2 A_{mn}^2 \qquad (A.2.13)$$

To find the value of any coefficient A_{mn} in the series consider the change in strain energy δU due to a change δA_{mn} in A_{mn}. Thus

$$\delta U = \frac{\pi^4 D}{8a^2} (n^2 + m^2)^2 \cdot 2A_{mn}\, \delta A_{mn} \qquad (A.2.14)$$

Now consider the work done on the panel by the pressure due to a change of δA_{mn}. The change in deflection is

$$\delta w = \delta A_{mn} \sin\left(\frac{n\pi x}{a}\right) \sin\left(\frac{m\pi y}{a}\right) \qquad (A.2.15)$$

Thus the work done is

$$\delta W = \int p \, \delta w \, dA$$

$$= p \, \delta A_{mn} \int_{x=0}^{a} \int_{y=0}^{a} \sin\left(\frac{n\pi x}{a}\right) \sin\left(\frac{m\pi y}{a}\right) dy \, dx$$

Now,
$$\int_{x=0}^{a} \sin\left(\frac{n\pi x}{a}\right) dx = \frac{2a}{n\pi} \quad , \qquad n \text{ odd}$$
$$= 0 \quad , \qquad n \text{ even}$$

$$\therefore \quad \delta W = p \, \delta A_{mn} \frac{4a^2}{nm\pi^2} \quad , \qquad n,m \text{ odd}$$
$$= 0 \quad , \qquad n.m \text{ even} \tag{A.2.16}$$

By Castigliano $\delta W = \delta U$, thus equating (A.2.14) and (A.2.16)

$$A_{mn} = \frac{16pa^4}{\pi^6 D} \frac{1}{n \, m \, (n^2+m^2)^2} \qquad n,m \text{ odd} \tag{A.2.17}$$

Hence, the Navier-Stokes solution is

$$w = \frac{16pa^4}{\pi^6 D} \sum_{}^{\infty} \sum_{}^{\infty} \frac{\sin\left(\frac{n\pi x}{a}\right) \sin\left(\frac{m\pi y}{a}\right)}{n \, m \, (n^2+m^2)^2} \qquad n,m \text{ odd} \tag{A.2.18}$$

A.3.O ORTHOTROPIC PLATE THEORY

A.3.1 General Equations

The following analysis has been developed from Reference 8. Consider a panel, using the same notation as in Appendix 2. For the purpose of this analysis it is assumed that the panel has elastic properties which are symmetrical about the co-ordinate planes. Then four constants, E_x', E_y' E'' and G are needed to define the stress components as

$$
\left.
\begin{aligned}
\sigma_x &= E_x' \, \epsilon_x + E'' \, \epsilon_y \\[2ex]
\sigma_y &= E_y' \, \epsilon_y + E'' \, \epsilon_x \\[2ex]
\sigma_{xy} &= G \, \gamma_{xy} = 2 \, G \, \epsilon_{xy}
\end{aligned}
\right\}
\tag{A.3.1}
$$

The components of strain are

$$
\epsilon_x = - z \, \frac{\partial^2 w}{\partial x^2} \quad, \quad \epsilon_y = - z \, \frac{\partial^2 w}{\partial y^2} \quad, \quad \gamma_{xy} = - 2z \, \frac{\partial^2 w}{\partial x \partial y}
\tag{A.3.2}
$$

Hence the corresponding stress components from (A.3.1) are

$$
\left.
\begin{aligned}
\sigma_x &= - z \left[E_x' \, \frac{\partial^2 w}{\partial x^2} + E'' \, \frac{\partial^2 w}{\partial y^2} \right] \\[2ex]
\sigma_y &= - z \left[E_y' \, \frac{\partial^2 w}{\partial y^2} + E'' \, \frac{\partial^2 w}{\partial x^2} \right] \\[2ex]
\sigma_z &= - z \, 2G \, \frac{\partial^2 w}{\partial x \partial y}
\end{aligned}
\right\}
\tag{A.3.3}
$$

Using these expressions the stress components for bending and twisting moments are

$$
\left.
\begin{aligned}
M_x &= \int_{-t/2}^{t/2} \sigma_x \, z \, dZ = - \left[D_x \, \frac{\partial^2 w}{\partial x^2} + D_1 \, \frac{\partial^2 w}{\partial y^2} \right] \\[2ex]
M_y &= \int_{-t/2}^{t/2} \sigma_y \, z \, dZ = - \left[D_y \, \frac{\partial^2 w}{\partial y^2} + D_1 \, \frac{\partial^2 w}{\partial x^2} \right] \\[2ex]
M_{xy} &= - \int_{-t/2}^{t/2} \tau_{xy} \, z \, dZ = 2D_{xy} \, \frac{\partial^2 w}{\partial x \partial y}
\end{aligned}
\right\}
\tag{A.3.4}
$$

where

$$D_x = \frac{E'_x t^3}{12}, \quad D_y = \frac{E'_y t^3}{12}, \quad D_1 = \frac{E''t^3}{12}, \quad D_{xy} = \frac{Gt^3}{12} \tag{A.3.5}$$

and $\frac{t^3}{12}$ is the second moment of area of the slab per unit width, 'I'.

Substituting (A.3.4) into the differential equation for equilibrium (A.2.7) we obtain

$$D_x \frac{\partial^4 w}{\partial x^4} + 2(D_1 + 2D_{xy}) \frac{\partial^4 w}{\partial x^2 \partial y^2} + D_y \frac{\partial^4 w}{\partial y^4} = p \tag{A.3.6}$$

or

$$D_x \frac{\partial^4 w}{\partial x^4} + 2H \frac{\partial^4 w}{\partial x^2 \partial y^2} + D_y \frac{\partial^4 w}{\partial y^4} = p \tag{A.3.7}$$

A.3.2 Application to Reinforced Concrete

A simple analysis for reinforced concrete was developed by Reference 8. as follows.

In terms of the elastic constants of (A.3.5) we have approximately

$$\nu_c = \frac{E''}{\sqrt{E'_x E'_y}}$$

For a slab with reinforcement in the x and y directions we then have, in terms of rigidities of equivalent concrete panels,

$$\left. \begin{aligned}
D_x &= \frac{E_c}{1-\nu_c^2} \left[I_{cx} + \left(\frac{E_s}{E_c} - 1 \right) I_{sx} \right] \\[2mm]
D_y &= \frac{E_c}{1-\nu_c^2} \left[I_{cy} + \left(\frac{E_s}{E_c} - 1 \right) I_{sy} \right] \\[2mm]
D_1 &= \nu_c \sqrt{D_x D_y} \\[2mm]
D_{xy} &= \frac{1-\nu_c}{2} \sqrt{D_x D_y}
\end{aligned} \right\} \tag{A.3.8}$$

where I_{cx}, I_{cy} and I_{sx}, I_{sy} are second moments of area about orthogonal axes, of the conrete and steel respectively. The expression for D_{xy} is also recommended by Reference 8. Substitution into (A.3.7) leads to

$$D_x \frac{\partial^4 w}{\partial x^4} + 2 \sqrt{D_x D_y} \frac{\partial^4 w}{\partial x^2 \partial y^2} + D_y \frac{\partial^4 w}{\partial y^4} = p \tag{A.3.9}$$

A solution to (A.3.7) can be developed from a Fourier Series in a similar way to the Navier-Stokes solution in Appendix 2. The solution for a square panel of side a becomes
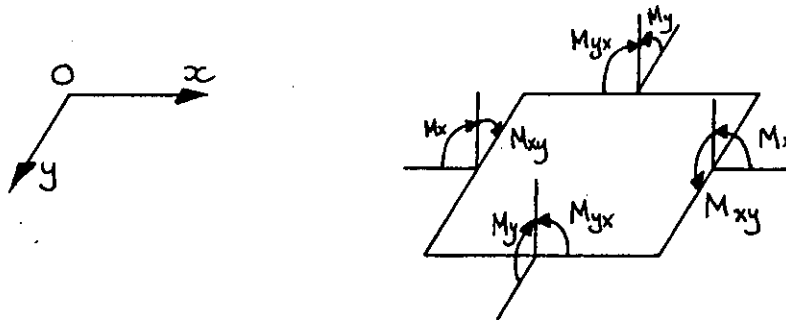
$$w = \frac{16pa^4}{\pi^6} \sum_{n=1}^{\infty} \sum_{m=1}^{\infty} \frac{\sin\left(\frac{n\pi x}{a}\right) \sin\left(\frac{m\pi y}{a}\right)}{n \, m \, (n^4 D_x + 2n^2 m^2 H + m^4 D_y)} \quad n,m \text{ odd} \tag{A.3.10}$$

Now, by substituting

$$D_y = \lambda D_x \qquad \text{where } \lambda > 1$$

and

$$H = \sqrt{D_x D_y}$$

Then

$$w = \frac{16a^4 p}{\pi^6 D_x} \sum_{n=1}^{\infty} \sum_{m=1}^{\infty} \frac{\sin\left(\frac{n\pi x}{a}\right) \sin\left(\frac{m\pi y}{a}\right)}{n \, m \, (n^2 + \lambda m^2)^2} \tag{A.3.11}$$

or

$$w = \frac{16a^4 p}{\pi^6 D_x} k_i' \tag{A.3.12}$$

Finally, note that when $\lambda = 1$, the Navier-Stokes solution (A.2.18) for an isotropic panel is returned.
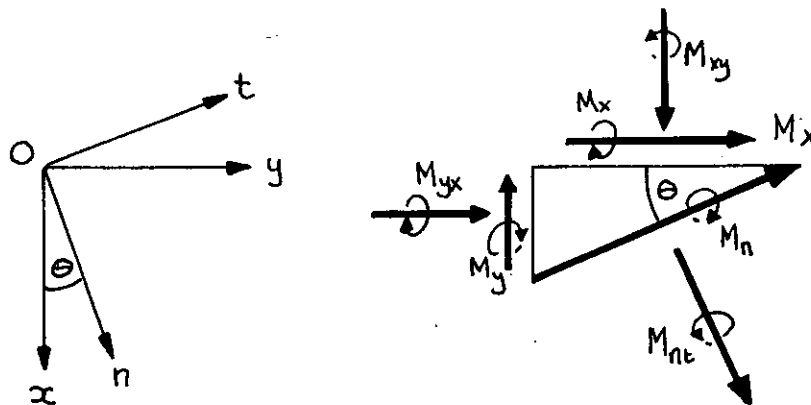
A.4.0 THE PLANE MOMENT SYSTEM

A.4.1 Resolution of Moments - Principal Moments

Adopting the convention shown above, the twisting moments vectors are positive along the outward normal.

The moments acting along a line whose normal makes an angle θ with the x-axis can be determined by consideration of the triangular plate element shown below.

Noting that moments are per unit length, then resolving moments vectors along Ot gives

$$M_n = (M_x \cos\theta) \cos\theta + (M_y \sin\theta) \sin\theta + (M_{yx} \sin\theta) \cos\theta$$

$$- (M_{xy} \cos\theta) \sin\theta$$

$$= M_x \cos^2\theta + M_y \sin^2\theta - 2M_{xy} \sin\theta \cos\theta \qquad (A.4.1)$$

since $M_{xy} = - M_{yx}$

A corresponding diagram can be drawn for M_t, or by putting $\theta = 90^{\circ} + \theta$ and replacing M_n by M_t in (A.4.1).

$$M_t = M_x \sin^2\theta + M_y \cos^2\theta + 2M_{xy} \sin\theta \cos\theta \qquad (A.4.2)$$

Resolving parallel with O_n,

$$M_{nt} = (M_x \cos\theta) \sin\theta - (M_y \sin\theta) \cos\theta + (M_{xy} \cos\theta) \cos\theta$$
$$+ (M_{yx} \sin\theta) \sin\theta$$

$$= (M_x - M_y) \sin\theta \cos\theta + M_{xy} (\cos^2\theta - \sin^2\theta)$$

$$= (M_x - M_y) \sin 2\theta + M_{xy} \cos 2\theta \qquad \text{(A.4.3)}$$

These equations are similar to those of a plane stress system since the moment system is derived from the integration of the stress (times a lever) through the depth.

There are two orthogonal directions of principal moments corresponding to those at which the twisting moment $M_{nt} = 0$. This occurs when

$$\tan 2\theta = \frac{M_{xy}}{M_y - M_x} \qquad \text{(A.4.4)}$$

The plane moment field system is best defined in terms of the Principal Moments.

A.4.2 Principal Moment Fields

The Navier-Stokes solution,

$$w = \frac{16a^4 p}{\pi^6 D} \sum_{n=1}^{\infty} \sum_{m=1}^{\infty} \frac{\sin\left(\frac{n\pi x}{a}\right) \sin\left(\frac{m\pi x}{a}\right)}{n\, m\, (n^2 + m^2)^2} \qquad n, m \text{ odd}$$

was used to calculate the principal moment system as follows.

From equations (A.2.5)

$$M_x = -D \left[\frac{\partial^2 w}{\partial x^2} + \nu \frac{\partial^2 w}{\partial y^2} \right]$$

$$M_y = -D \left[\frac{\partial^2 w}{\partial y^2} + \nu \frac{\partial^2 w}{\partial x^2} \right]$$

$$M_{xy} = D (1-\nu) \frac{\partial^2 w}{\partial x \partial y}$$

Then

$$M_x = \frac{16pa^2}{\pi^4} \sum_{n=1}^{\infty} \sum_{m=1}^{\infty} (n^2 + \nu m^2) \left\{ \frac{\sin\left(\frac{n\pi x}{a}\right) \sin\left(\frac{m\pi y}{a}\right)}{n\, m\, (n^2 + m^2)^2} \right\} \qquad \text{(A.4.5)}$$

$$M_y = \frac{16pa^2}{\pi^4} \sum_{n=1}^{\infty} \sum_{m=1}^{\infty} (m^2 + \nu n^2) \left\{ \frac{\sin\left(\frac{n\pi x}{a}\right) \sin\left(\frac{m\pi y}{a}\right)}{n\, m\, (n^2 + m^2)^2} \right\} \qquad \text{(A.4.6)}$$

$$M_{xy} = \frac{16pa^2}{\pi^4} (1-\nu) \sum_{n=1}^{\infty} \sum_{m=1}^{\infty} \frac{\cos\left(\frac{n\pi x}{a}\right) \cos\left(\frac{m\pi y}{a}\right)}{(n^2 + m^2)^2} \quad n,m \text{ odd} \qquad (A.4.7)$$

Using equation (A.4.4) the direction of the principal moments, θ, was calculated and this value substituted into equations A.4.1 and A.4.2 to obtain their magnitude. This was done by computer so that a diagram of the moment fields could be drawn as Figure 8.

A.5   TEST-PIECE DATA

Wiremesh

Type :-   19g galvanised welded square steel mesh at nominal ½ in. spacing.

Measurement :-

Wire Diameter   =   0.89 mm beneath galvanising

Strand Spacing   =   12.7   mm

Mass   =   1.002 kg / m^2 per layer

Tensile Tests :-   See Figure 2

Yield Strength   =   360 N/mm^2 at 0.004 strain

Ultimate Strength =   430 N/mm^2 at 0.110 strain

Premature failure was frequent at welds at 0.030 strain.

Concrete

Sand : Cement : Water Ratio   =   4.50 : 2.25 : 1

Cement :- Ordinary Portland Cement

Sand :- Oven dried and sieved.   Mixed in proportions

Diameter (microns)	% by weight
2400 - 1180	10
1180 - 600	50
600 - 300	30
300 - 150	9
150 - 0	1

Details of individual concrete mix properties are included in panel data.

Panels

Summary:-

Panel Number	Mesh Layers (Tension : Compression)
1	1T0C
2	1T0C
3	1T1C
4	2T1C
5	2T1C
6	2T1C (Diagonal)
7	2T2C
8	3T2C

Details overleaf.

		PANEL 1			PANEL 2			PANEL 3		
a	(mm)	490			485			490		
ρ_c	(kg/m³)	2200			2160			2200		
t	(mm)	12.94 (±0.26)			13.25 (±0.24)			13.12 (±0.26)		
E_s	(kN/mm²)	145			145			145		
F_{cu}	N/mm²	38.4 (±2.2)			40.8 (±3.1)			53.0 (±0.27)		
E_c	(kN/mm²)	28.0			29.5			30.5		
m_s/m_c	(%)	3.3			3.2			6.8		
K_x	(mm⁻¹)	0.021			0.020			0.038		
DIRECTION		XX	YY	MEAN	XX	YY	MEAN	XX	YY	MEAN
d_c	(mm)	2.33	2.33	-	2.14	2.14	-	2.61	2.61	-
d_1	(mm)	2.77	3.88	(±0.51)	2.59	3.48	(0.14)	3.05	3.94	(0.26)
d_2	(mm)	-	-	-	-	-	-	10.59	9.70	(0.23)
I_u	(mm⁴/mm)	20.34	19.98	20.16	24.50	24.10	24.30	21.61	21.11	21.36
d_{nu}	(mm)	7.55	7.56	-	7.60	7.62	-	7.83	7.83	-
I_c	(mm⁴/mm)	3.78	2.95	3.36	4.22	3.51	3.86	3.76	3.19	3.47
d_{nc}	(mm)	10.91	11.03	-	11.21	11.31	-	11.11	11.11	-
M_u	(Nmm/mm)	203.6	180.7	192	214.0	195.7	204	242.5	242.5	242
d_n	(mm)	12.23	12.34	-	12.68	12.68	-	12.23	12.23	-
λ	(FAILURE MODE)	0			0			0		

		PANEL 4			PANEL 5			PANEL 6		
a	(mm)	485			485			485		
ρ_c	(kg/m³)	2200			2250			2130		
t	(mm)	13.35	(0.47)		13.25	(±0.25)		12.89	(±0.49)	
E_s	(kN/mm²)	145			145			145		
f_{cu}	(N/mm²)	49.3	(0.21)		43.3	(±2.1)		50.3	(±0.7)	
E_c	(kN/mm²)	31.0			31.0			32.0		
m_s/m_c	(%)	10.9			10.2			10.5		
K_x	(mm⁻¹)	0.057			0.058			0.058		
DIRECTION		XX	YY	MEAN	XX	YY	MEAN	XY	YX	MEAN
d_c	(mm)	3.00	3.00	-	2.92	2.92	-	2.30	2.30	-
d_1	(mm)	3.44	4.33	(±0.23)	3.36	4.25	(±0.14)	2.74	3.63	(±0.14)
d_2	(mm)	5.22	4.33	(±0.23)	5.14	4.25	(±0.14)	4.52	3.63	(±0.14)
d_3	(mm)	10.80	9.91	(±0.16)	10.71	9.70	(±0.10)	10.38	9.49	(±0.20)
I_u	(mm⁴/mm)	21.10	20.90	21.00	20.98	20.76	20.87	23.28	23.07	23.17
d_{nu}	(mm)	8.09	8.08	-	8.00	7.98	-	7.51	7.50	-
I_c	(mm⁴/mm)	5.35	5.32	5.33	5.33	5.3	5.32	5.70	5.67	5.68
d_{nc}	(mm)	10.89	10.82		10.79	10.72		10.43	10.37	-
M_u	(Nmm/mm)	383.1	404.3	393	373.0	398.3	385	393.0	412.0	403
d_n	(mm)	11.95	11.93		11.23	11.65		11.51	11.51	-
λ	(FAILURE MODE)	0.3			0.3			O (DIAGONAL ARRANGEMENT)		

		PANEL 7			PANEL 8		
a	(mm)	485			485		
ρ_c	(kg/m³)	2150			2200		
t	(mm)	13.27	(±0.28)		12.34	(±0.42)	
E_s	(kN/mm²)	145			145		
f_{cu}	(N/mm²)	48.5	(±3.9)		47.2	(±1.3)	
E_c	(kN/mm²)	31.0			31.0		
m_s/m_c	(%)	13.6			18.3		
K_x	(mm⁻¹)	0.078			0.102		
DIRECTION		XX	YY	MEAN	XX	YY	MEAN
d_c	(mm)	1.86	1.86	–	1.85	1.85	–
d_1	(mm)	2.30	3.19	(±0.26)	2.29	3.18	(±0.25)
d_2	(mm)	4.08	3.19	(±0.26)	4.07	3.18	(±0.25)
d_3	(mm)	8.49	9.38	(±0.22)	4.07	4.96	(±0.25)
d_4	(mm)	10.27	9.38	(±0.22)	7.89	8.78	(±0.29)
d_5	(mm)	–	–	–	9.67	8.78	(±0.29)
I_u	(mm⁴/mm)	27.79	27.89	27.84	21.85	21.61	21.75
d_{nu}	mm	7.49	7.49	–	6.97	6.99	–
I_c	(mm⁴/mm)	7.03	6.87	6.95	7.18	6.60	6.90
d_{nc}	(mm)	10.49	10.49	–	9.38	9.44	–
M_u	(Nmm/mm)	504.0	503.0	504	570.0	544.1	557
d_n	(mm)	11.36	11.36	–	10.21	10.13	–
λ	(FAILURE MODE)	0.5			0.6		

FIG. 1. LIMIT STATE STRESS BLOCKS

(a) HOGENSTEAD ET AL.

$\lambda_3 f_c'$

STRESS
(N/mm²)

STRAIN

$\epsilon_{cu} = 0.0035$

$\lambda_2 \times \epsilon_{cu}$

(b) CP 110

STRESS
(N/mm²)

$\frac{0.67}{\gamma_m} f_{cu}$ ($\gamma_m = 1.5$)

$4500 \, (f_{cu})^{1/2}$

$\frac{(f_{cu})^{1/2}}{5000}$

STRAIN

$\epsilon_{cu} = 0.0035$

(c) WITNEY

STRESS
(N/mm²)

$0.85 \, f_c'$

STRAIN

$\epsilon_{cu} = 0.0035$

(d) C.E.B.

STRESS
(N/mm²)

$0.85 \, f_c'$

0.002

STRAIN

$\epsilon_{cu} = 0.0035$
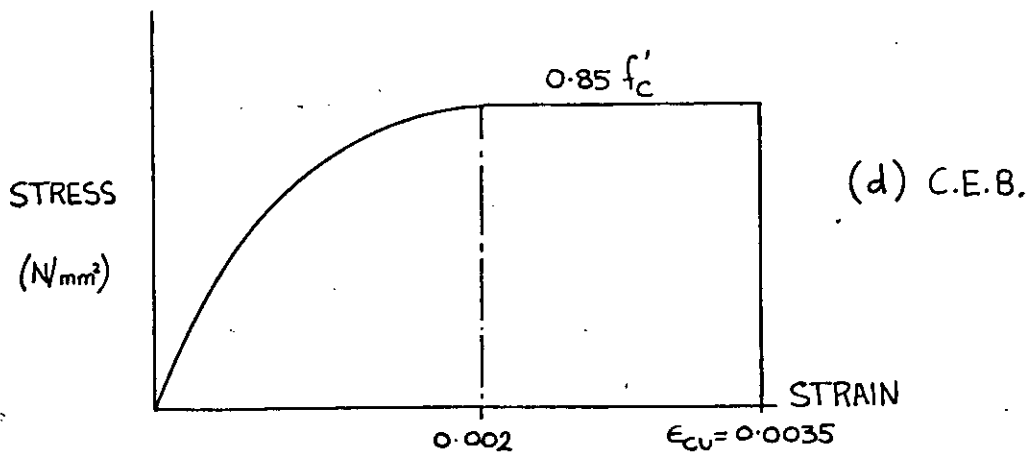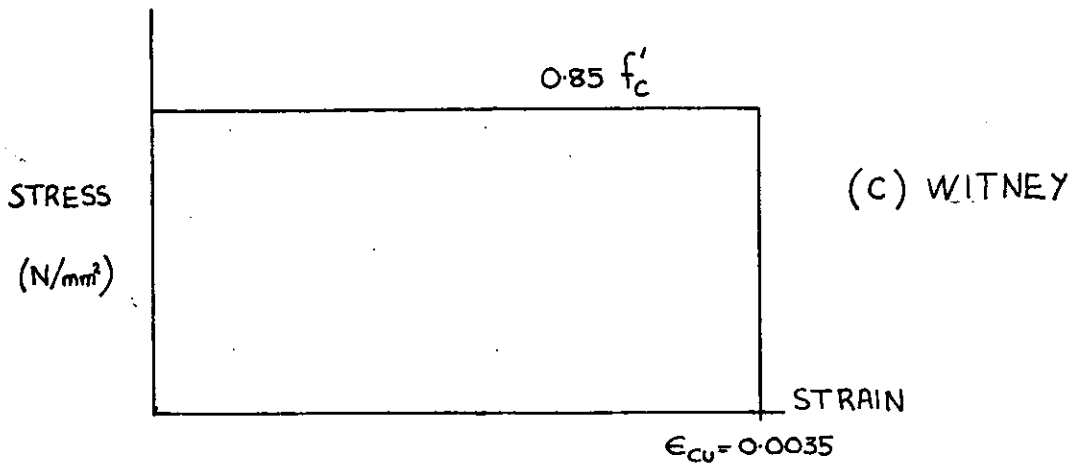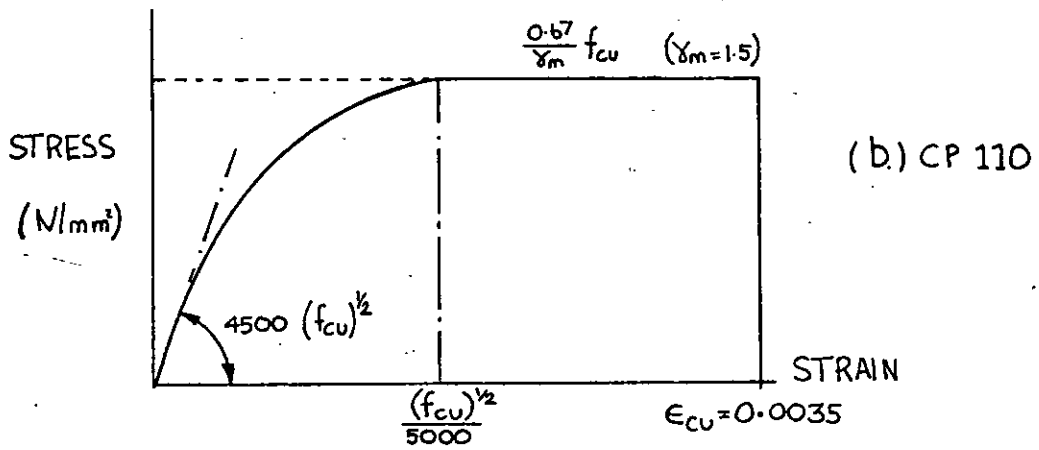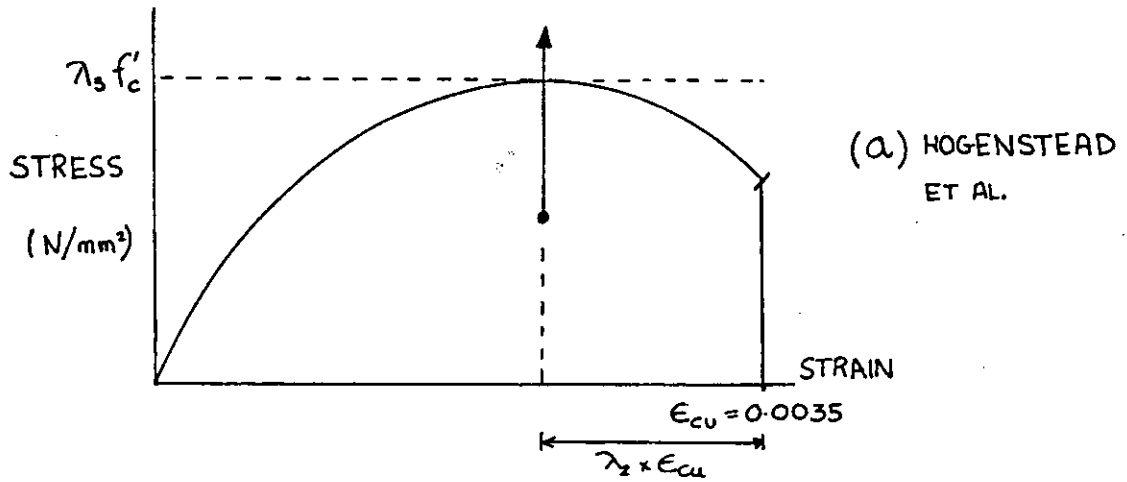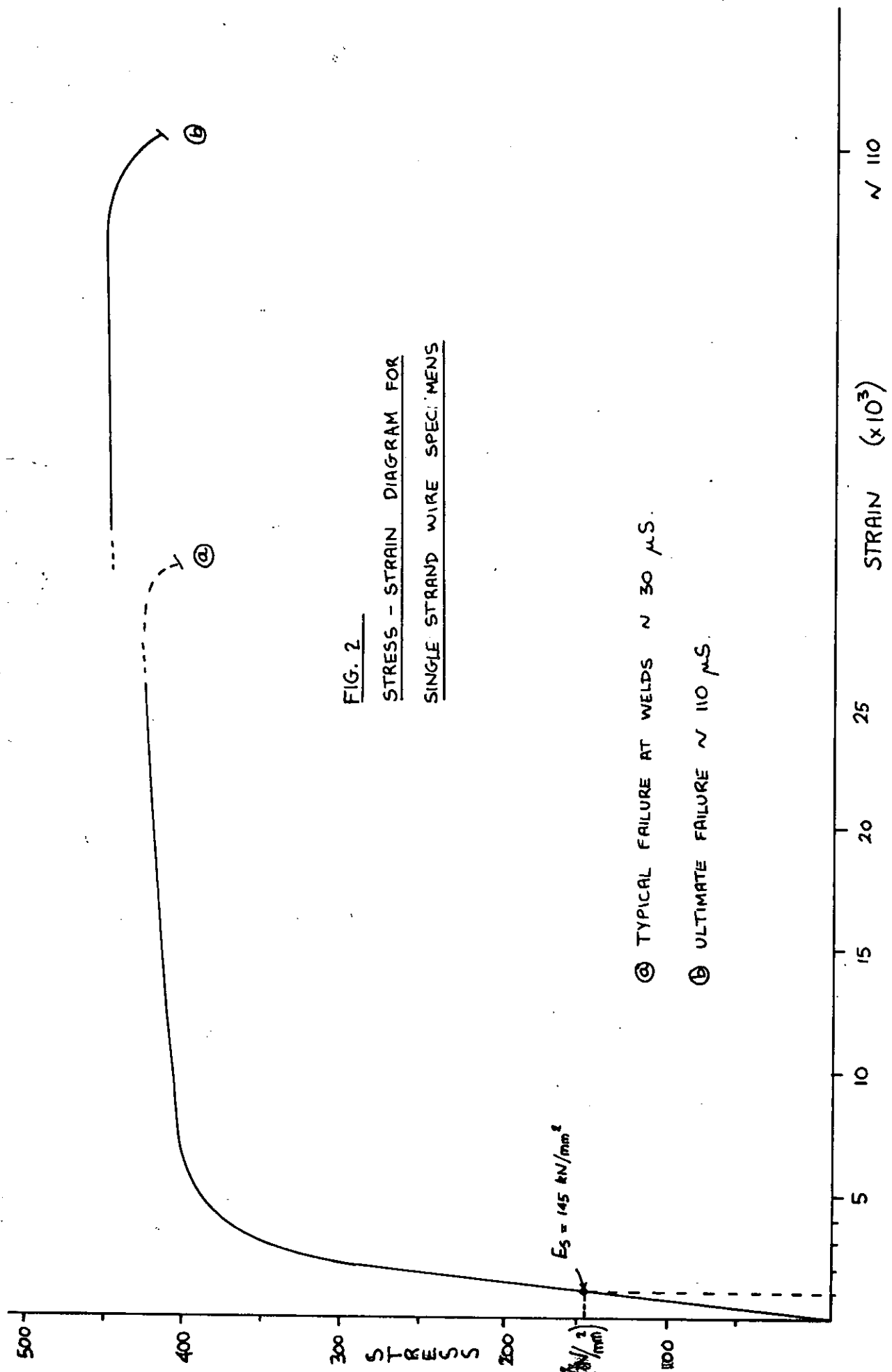
FIG. 2

STRESS – STRAIN DIAGRAM FOR
SINGLE STRAND WIRE SPECIMENS

ⓐ TYPICAL FAILURE AT WELDS ~ 30 μS.

ⓑ ULTIMATE FAILURE ~ 110 μS.
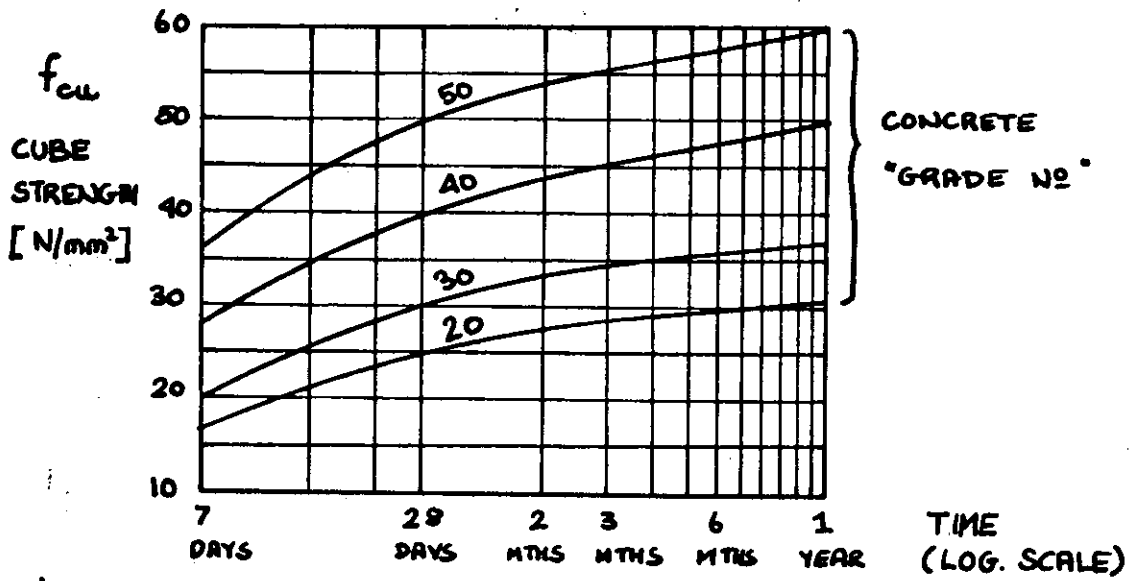
FIG. 3   VARIATION OF CUBE STRENGTH OF CONCRETE
WITH TIME (AND GRADE)   [REF. CP 110...]
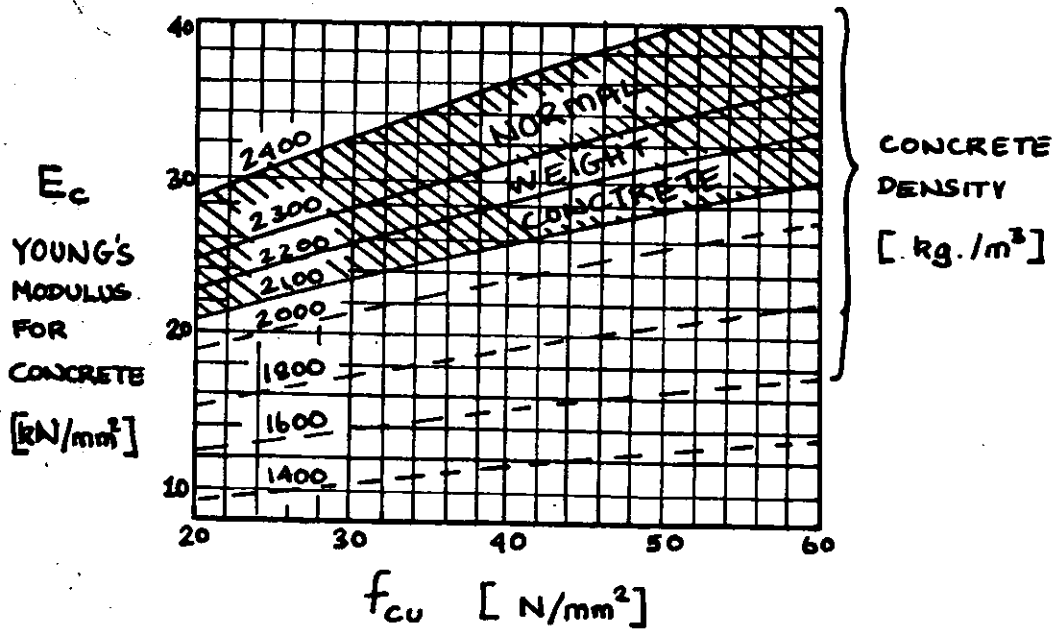
FIG. 4   VARIATION OF YOUNGS MODULUS OF CONCRETE
(COMPRESSION) WITH CUBE STRENGTH (f_{cu}) AND DENSITY
[REF. CP 110]
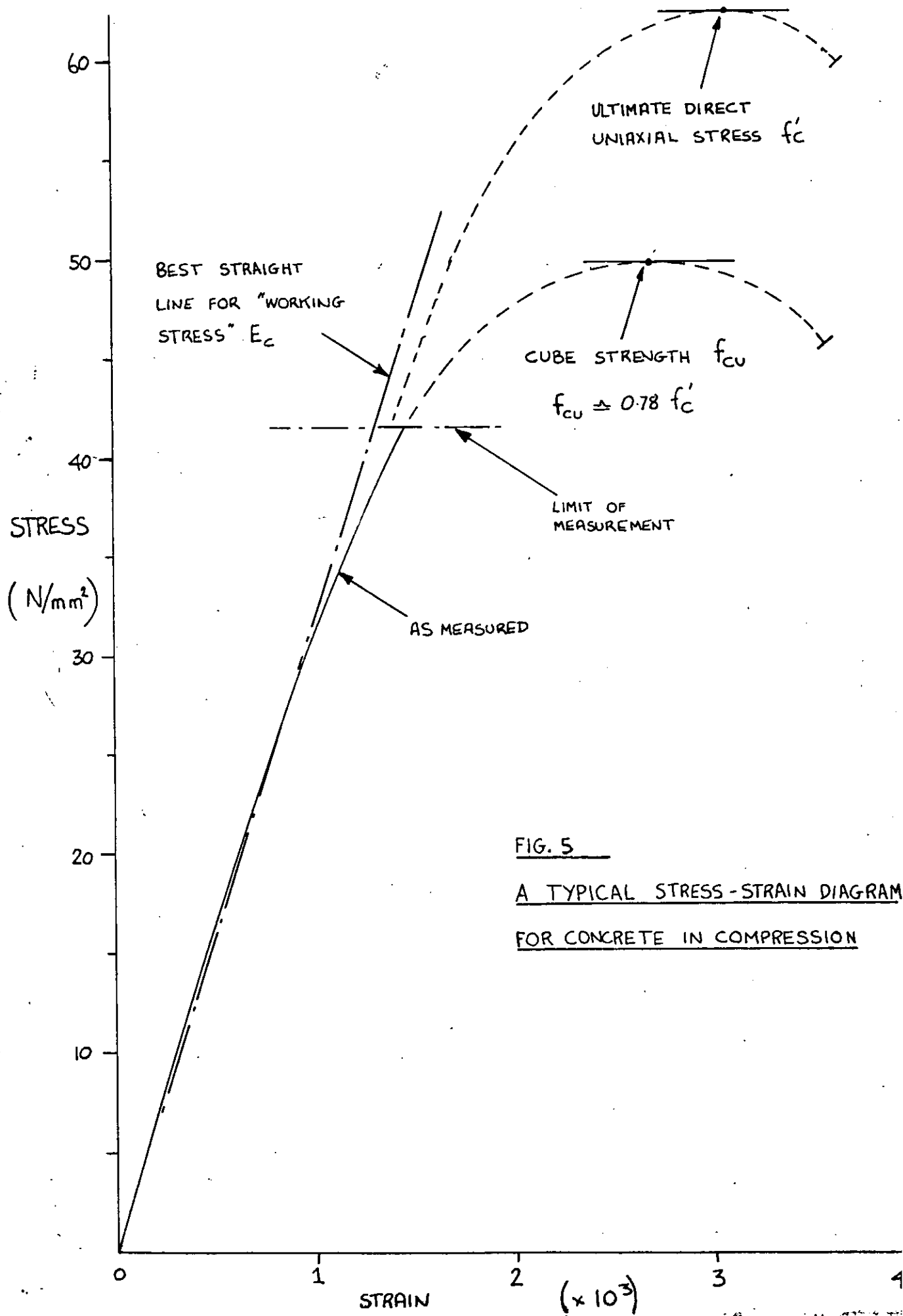
FIG. 5

A TYPICAL STRESS-STRAIN DIAGRAM

FOR CONCRETE IN COMPRESSION

FIG. 6   **THE NAVIER SOLUTION TO SIMPLY SUPPORTED PLATE UNDER**

UNIFORM LOADING – DEFLECTIONS

The Navier-Stokes solution is

$$w = \frac{16 a^4 p}{\pi^6 D} \sum_{m=1}^{\infty} \sum_{n=1}^{\infty} \frac{\sin\left(\frac{n\pi x}{a}\right) \sin\left(\frac{m\pi y}{a}\right)}{nm(n^2 + m^2)^2} \qquad n, m \text{ odd}.$$

$$\text{or} \qquad w = \frac{16 a^4 p}{\pi^6 D} k_i$$

The values of k_i were calculated for $(x/a, y/a)$ as follows ;

(x/a)	(y/a) .00	.05	.10	.15	.20	.25	.30	.35	.40	.45	.50
.05	.0068	.0790	.0193	.0247	.0293	.0332	.0363	.0385	.0398	.0402
.10		.0261	.0379	.0485	.0576	.0652	.0712	.0756	.0780	.0790
.15			.0551	.0705	.0839	.0950	.1038	.1102	.1140	.1153
.20				.0900	.1075	.1219	.1332	.1414	.1463	.1480
.25					.1281	.1453	.1589	.1687	.1746	.1765
.30						.1649	.1803	.1915	.1982	.2005
.35							.1973	.2005	.2169	.2194
.40								.2226	.2304	.2331
.45									.2413	.2413
.50										.2441

The table is symmetric about the diagonal.

Other important points are ;

x/a	y/a	k_i
1/3	1/3	0.1871
1/6	1/6	0.0663

FIG.7

ORTHOTROPIC PLATE THEORY

GRAPH TO SHOW VARIATION OF k_i' AT

VARIOUS $\left[\left(\frac{x}{a}\right) ; \left(\frac{y}{a}\right)\right]$ VALUES WITH λ,

WHERE k_i' GIVEN BY

$$W = \frac{16\,p\,a^4}{\pi^6\,D_x} \cdot k_i'\Bigg\}$$

AND $\qquad \lambda = D_y/D_x$

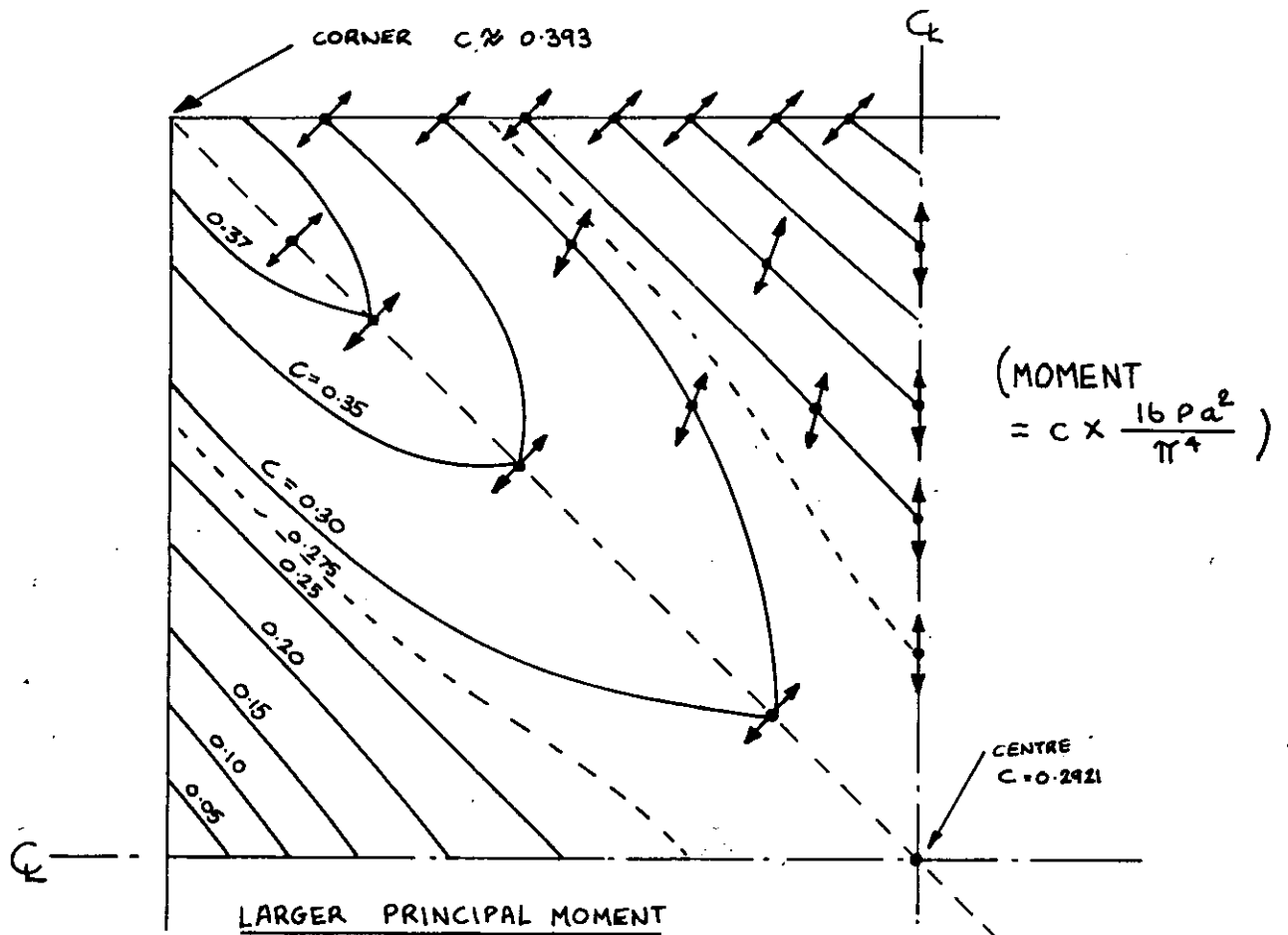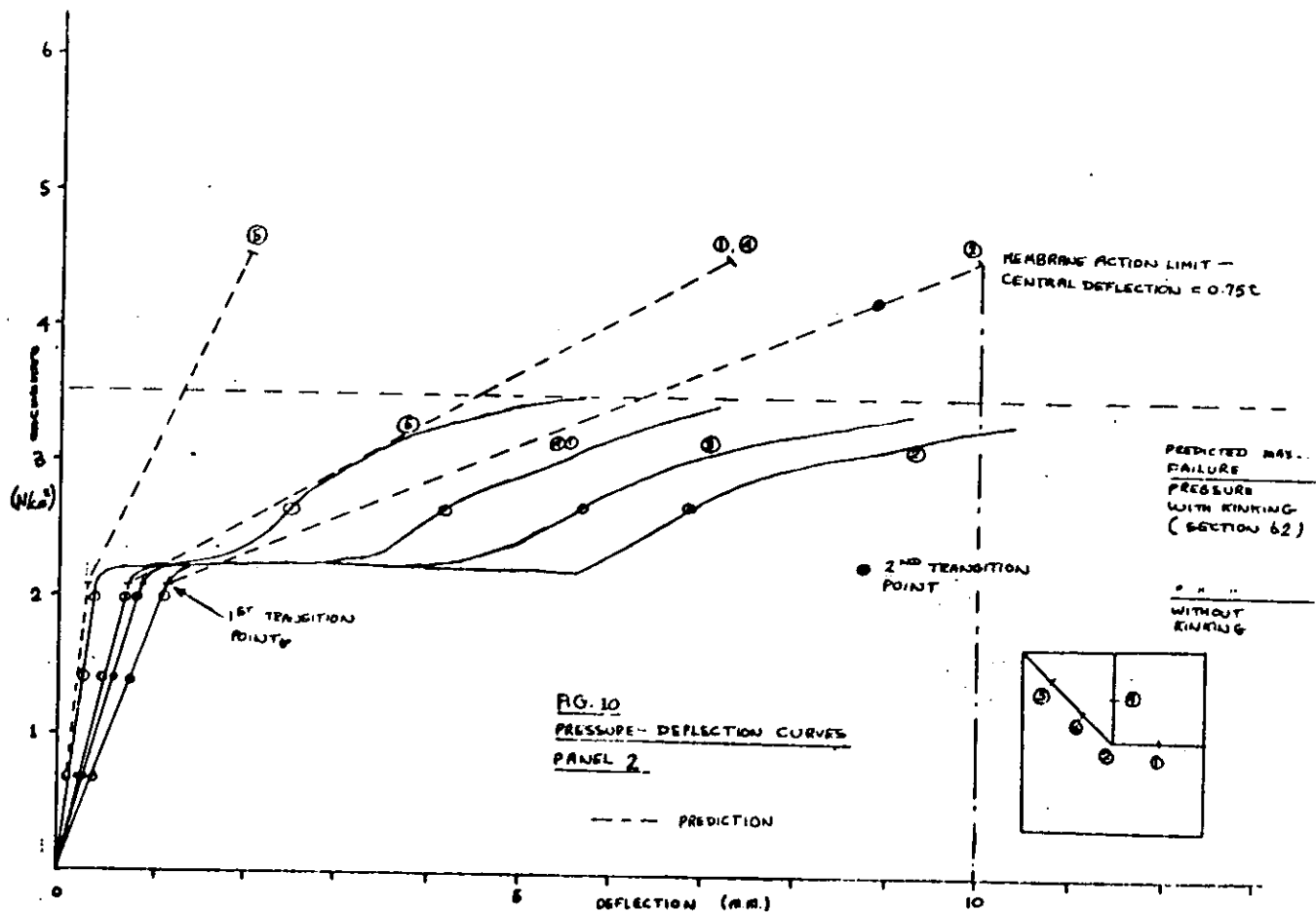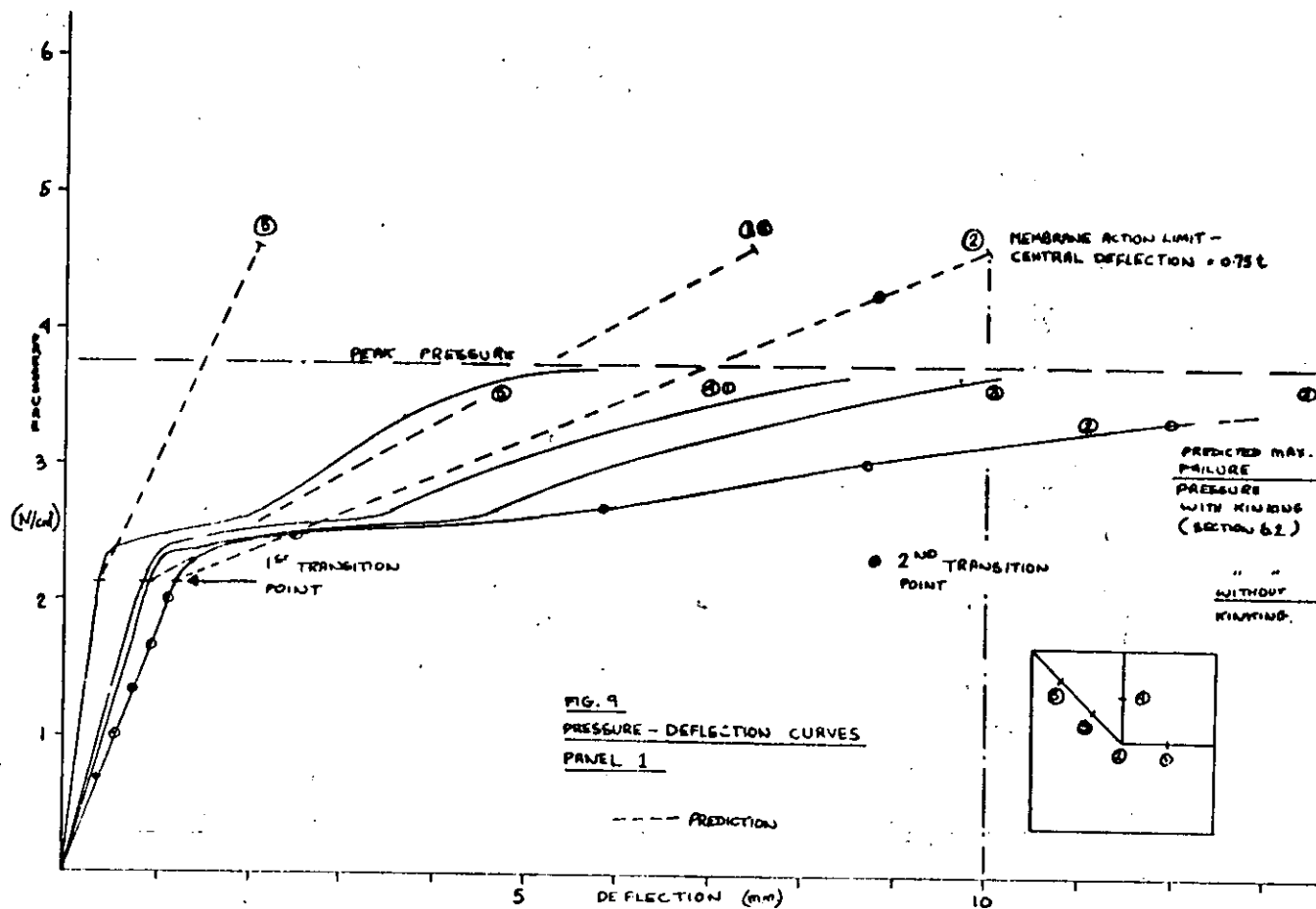$\left(\lambda = 1.0 \equiv \text{ISOTROPIC THEORY}\right)$
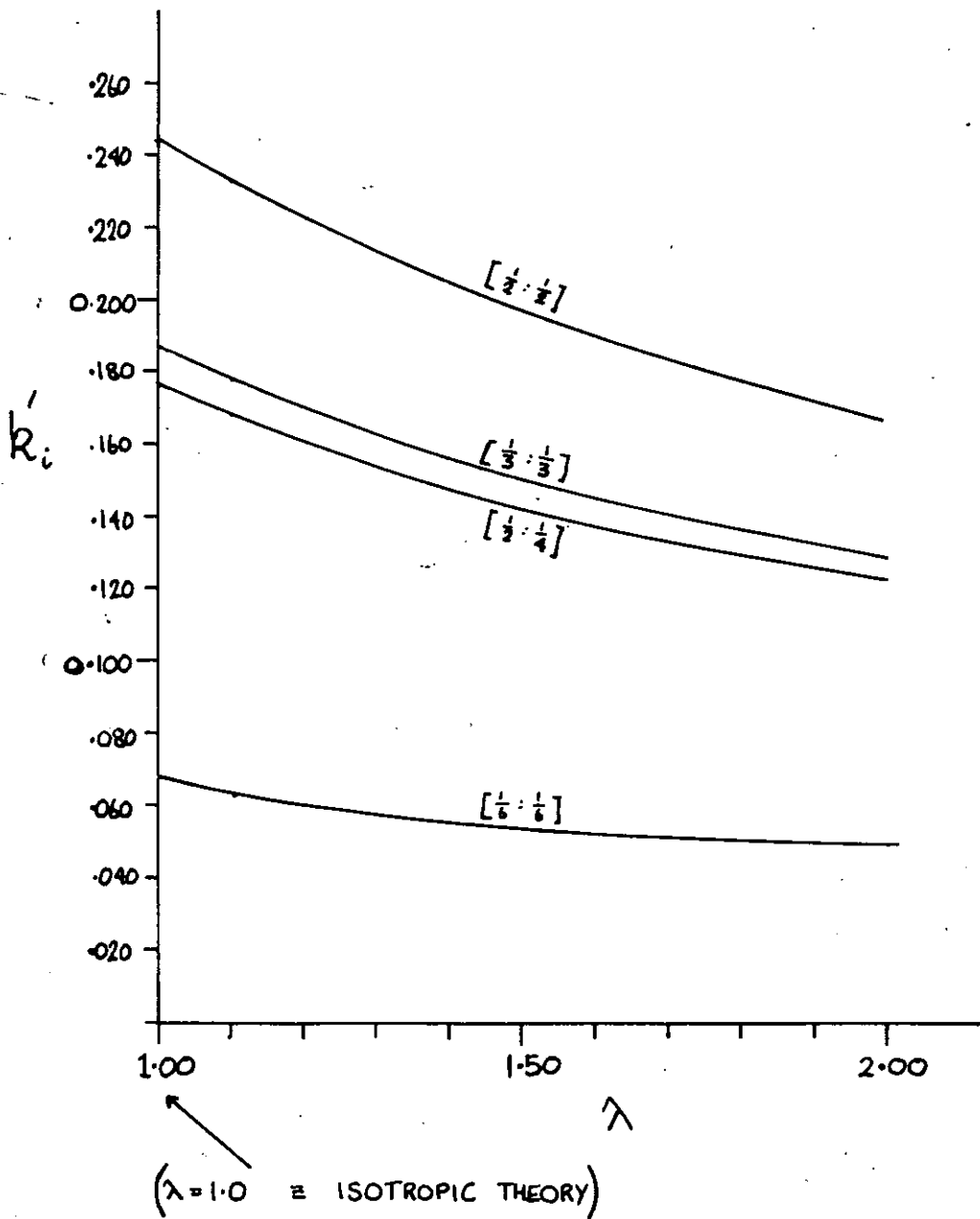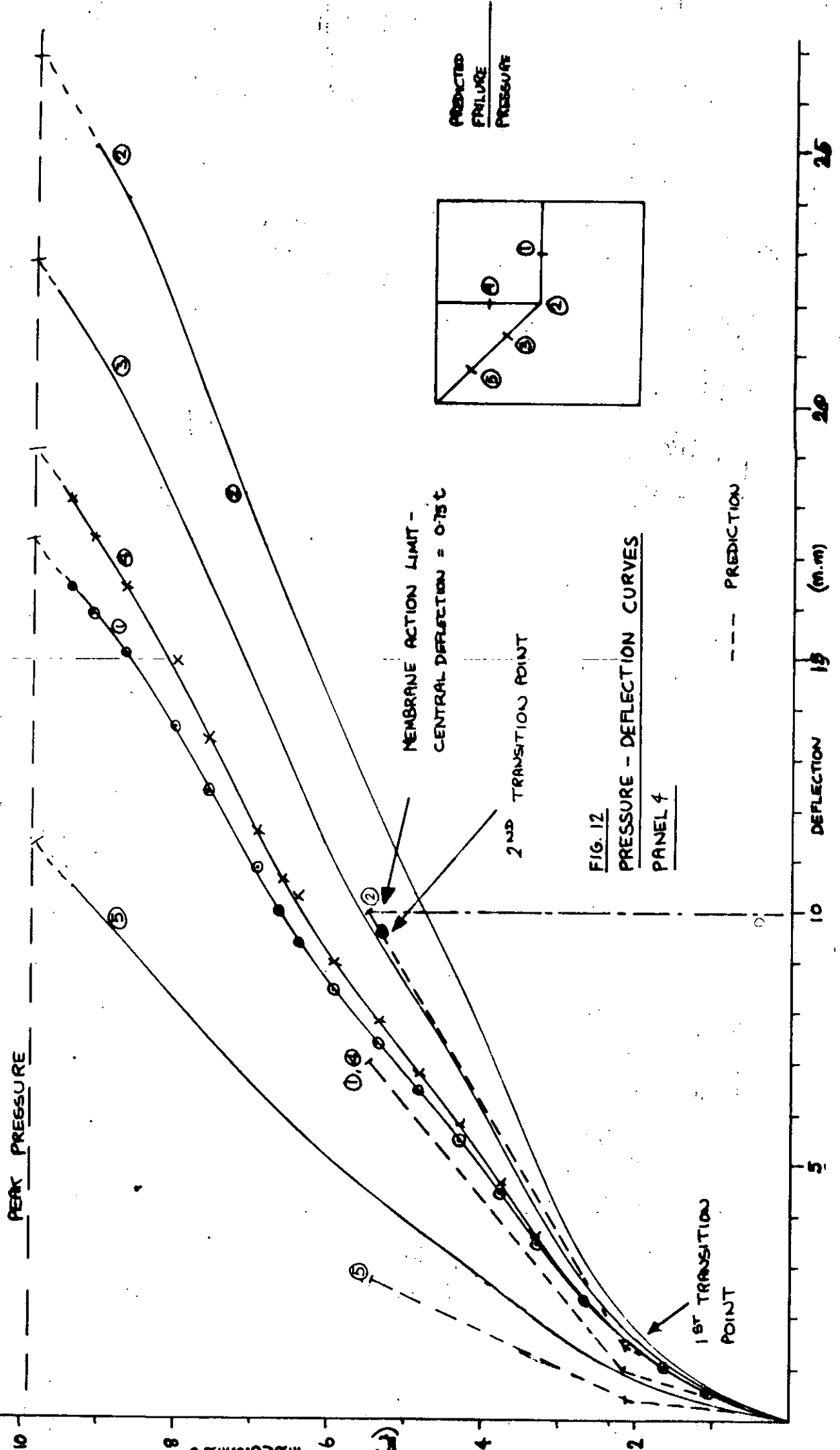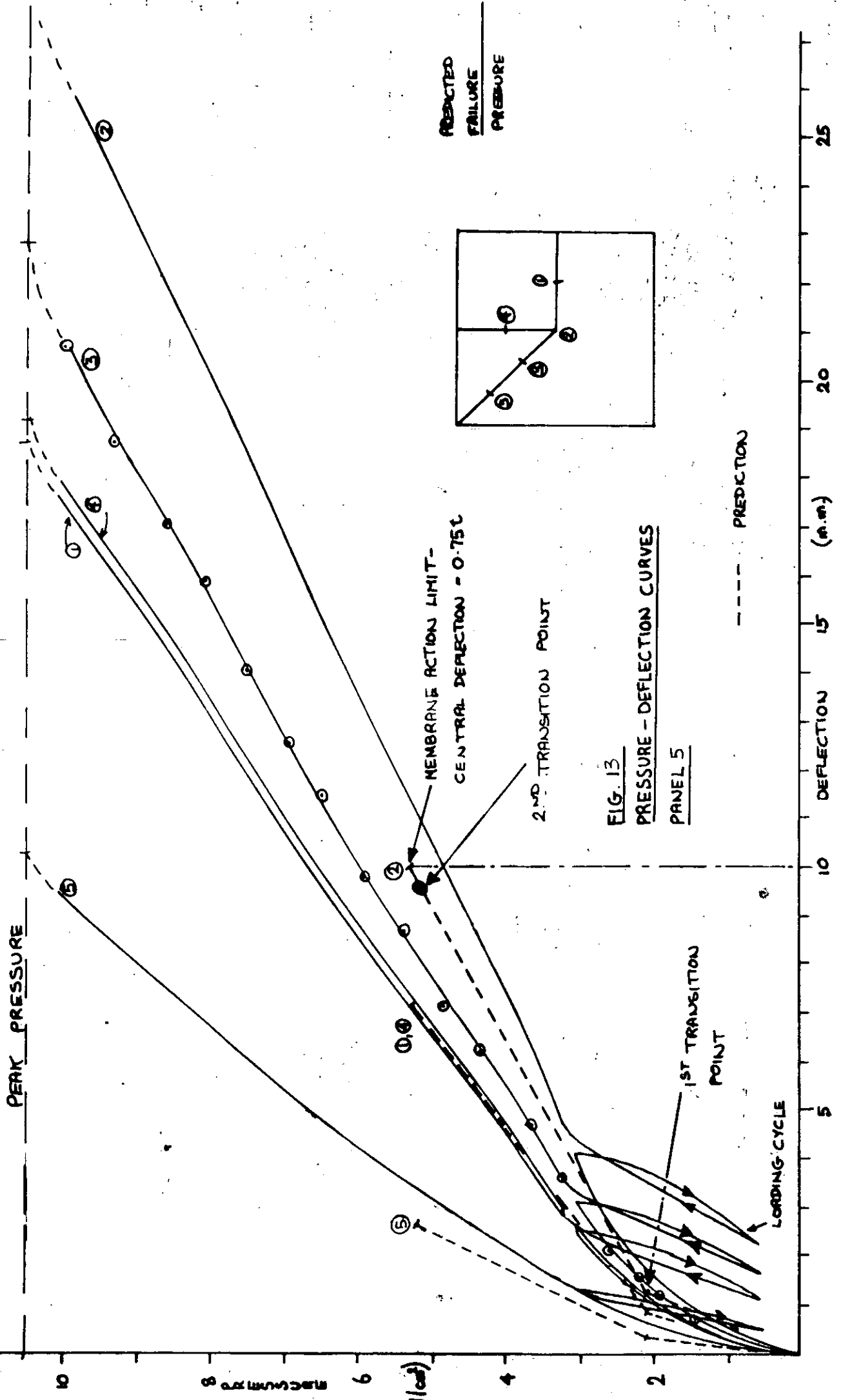
FIG. 8   CONTOURS AND DIRECTIONS OF PRINCIPAL MOMENTS

LARGER PRINCIPAL MOMENT

$$\left(\text{MOMENT} = c \times \frac{16\,P a^2}{\pi^4}\right)$$

SMALLER PRINCIPAL MOMENT

FIG. 9

PRESSURE – DEFLECTION CURVES

PANEL 1

– – – – PREDICTION

FIG. 10

PRESSURE – DEFLECTION CURVES

PANEL 2

– – – PREDICTION

FIG. 11

LOAD - DEFLECTION CURVES

PANEL 3

PEAK PRESSURE

PREDICTED
FAILURE
PRESSURE

MEMBRANE ACTION LIMIT -
CENTRAL DEFLECTION = 0.75 t

2ND TRANSITION POINT

1ST TRANSITION POINT
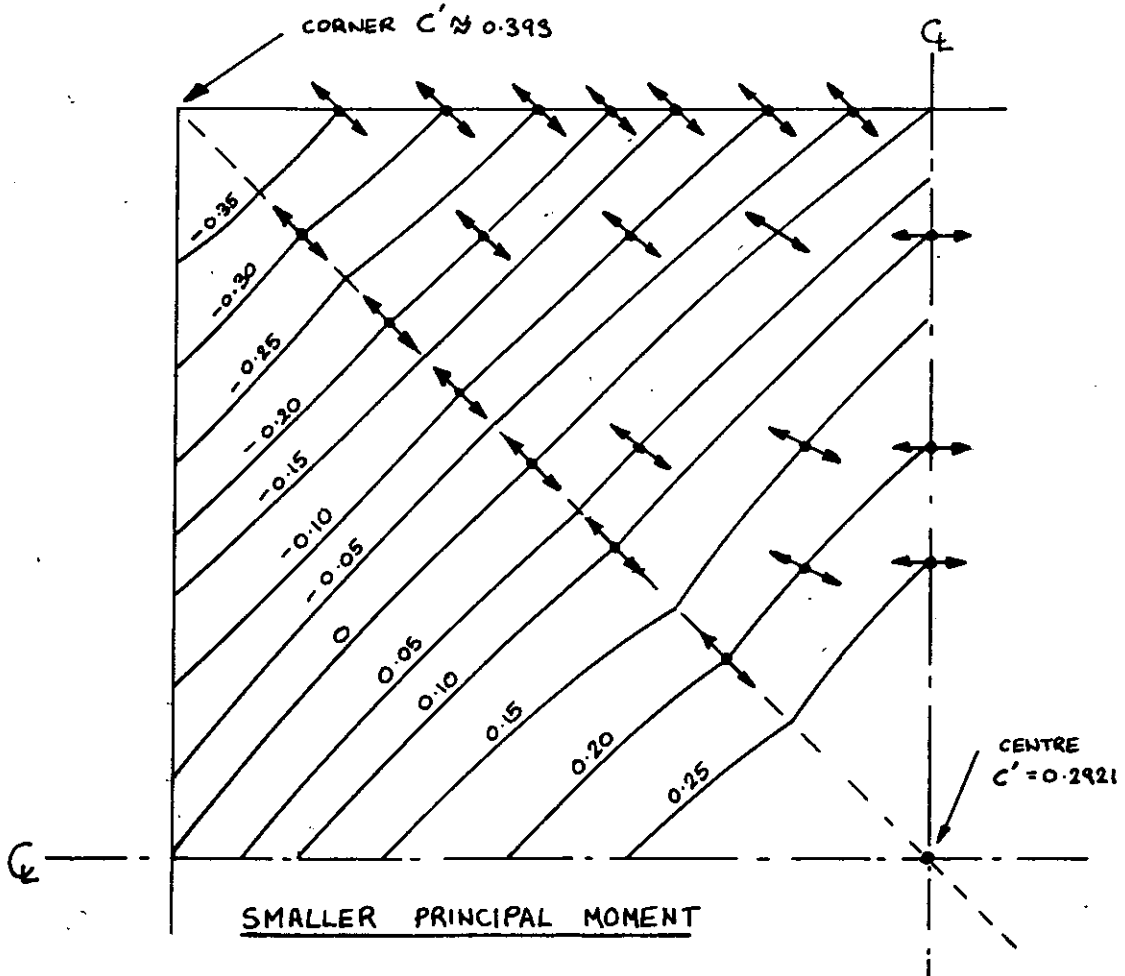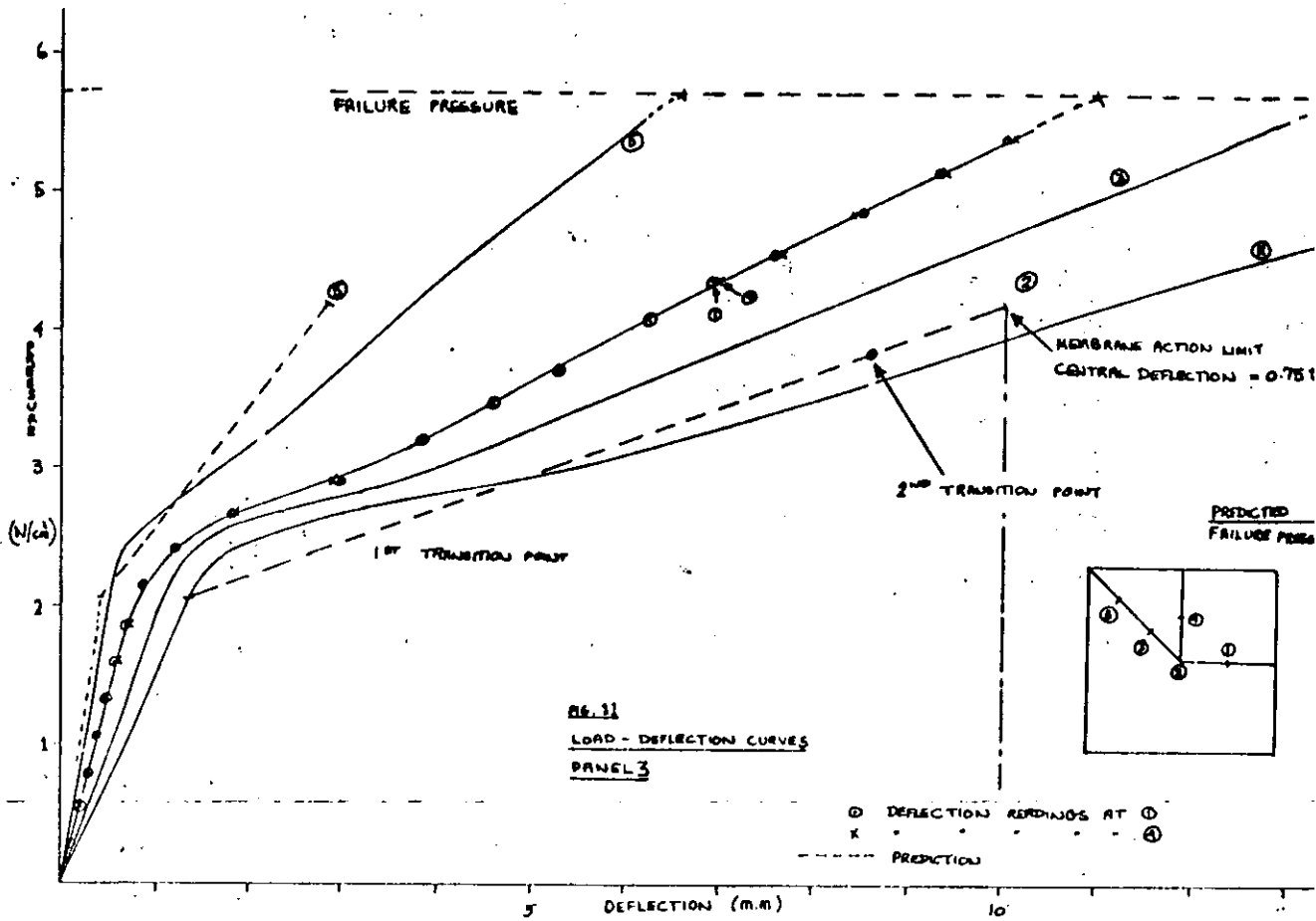
FIG. 12
PRESSURE - DEFLECTION CURVES
PANEL 4

--- PREDICTION
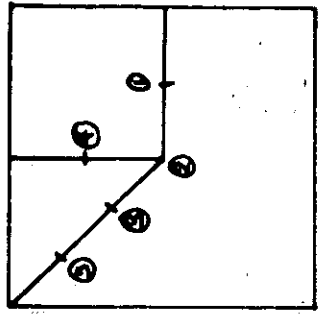
DEFLECTION (m.m)

FIG. 13
PRESSURE - DEFLECTION CURVES
PANEL 5

PEAK PRESSURE

PREDICTED FAILURE PRESSURE

MEMBRANE ACTION LIMIT - CENTRAL DEFLECTION = 0·75t

2ND TRANSITION POINT

1ST TRANSITION POINT

LOADING CYCLE

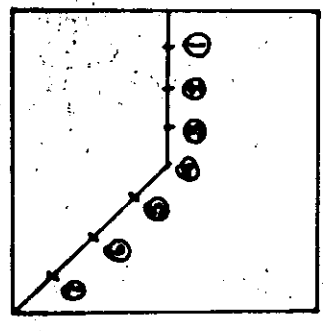---- PREDICTION
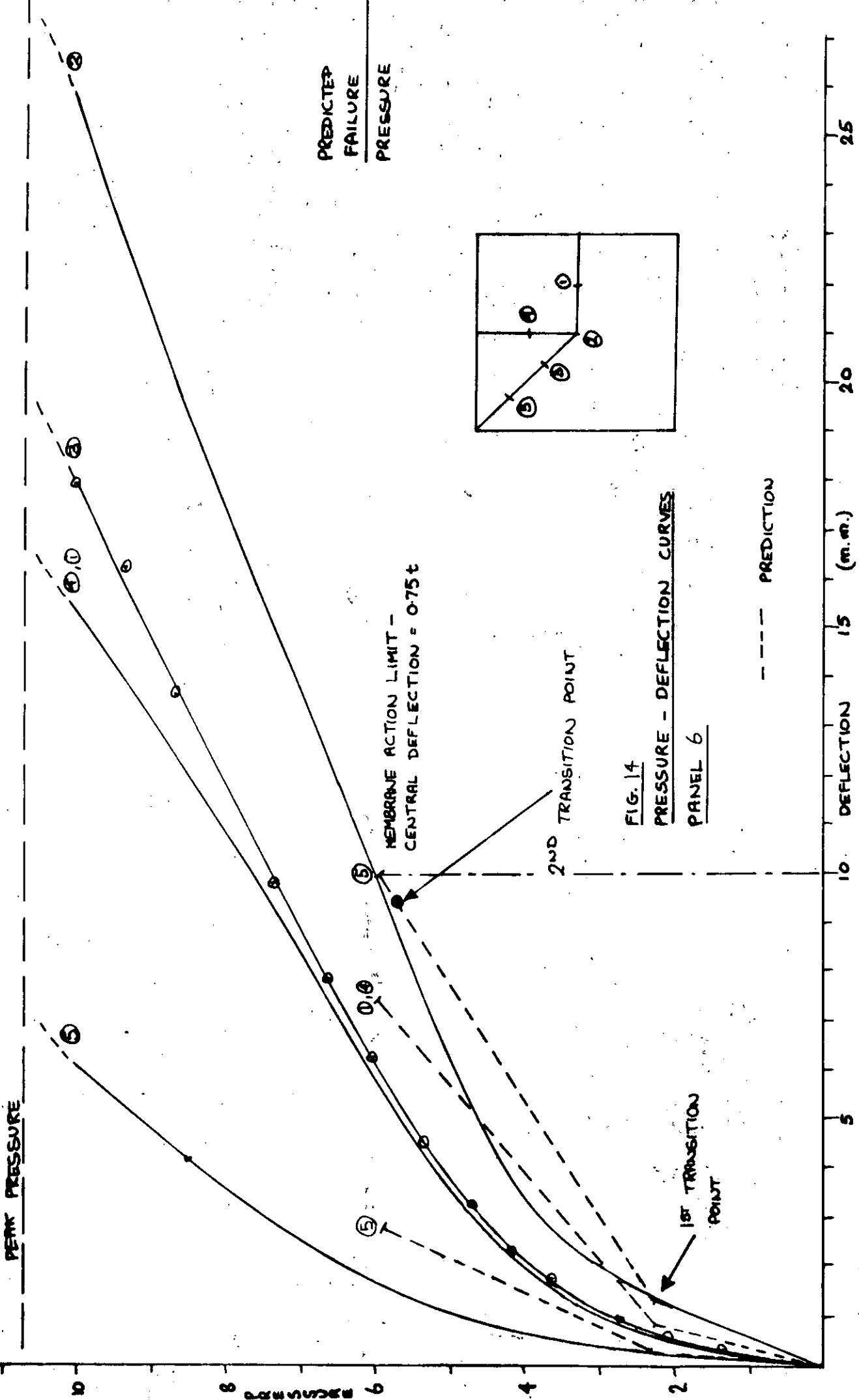
DEFLECTION (m.m.)

FIG. 14

PRESSURE - DEFLECTION CURVES

PANEL 6
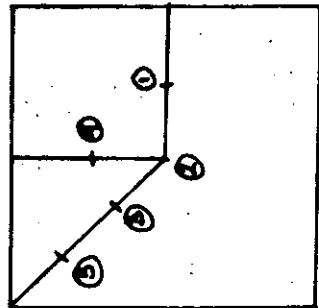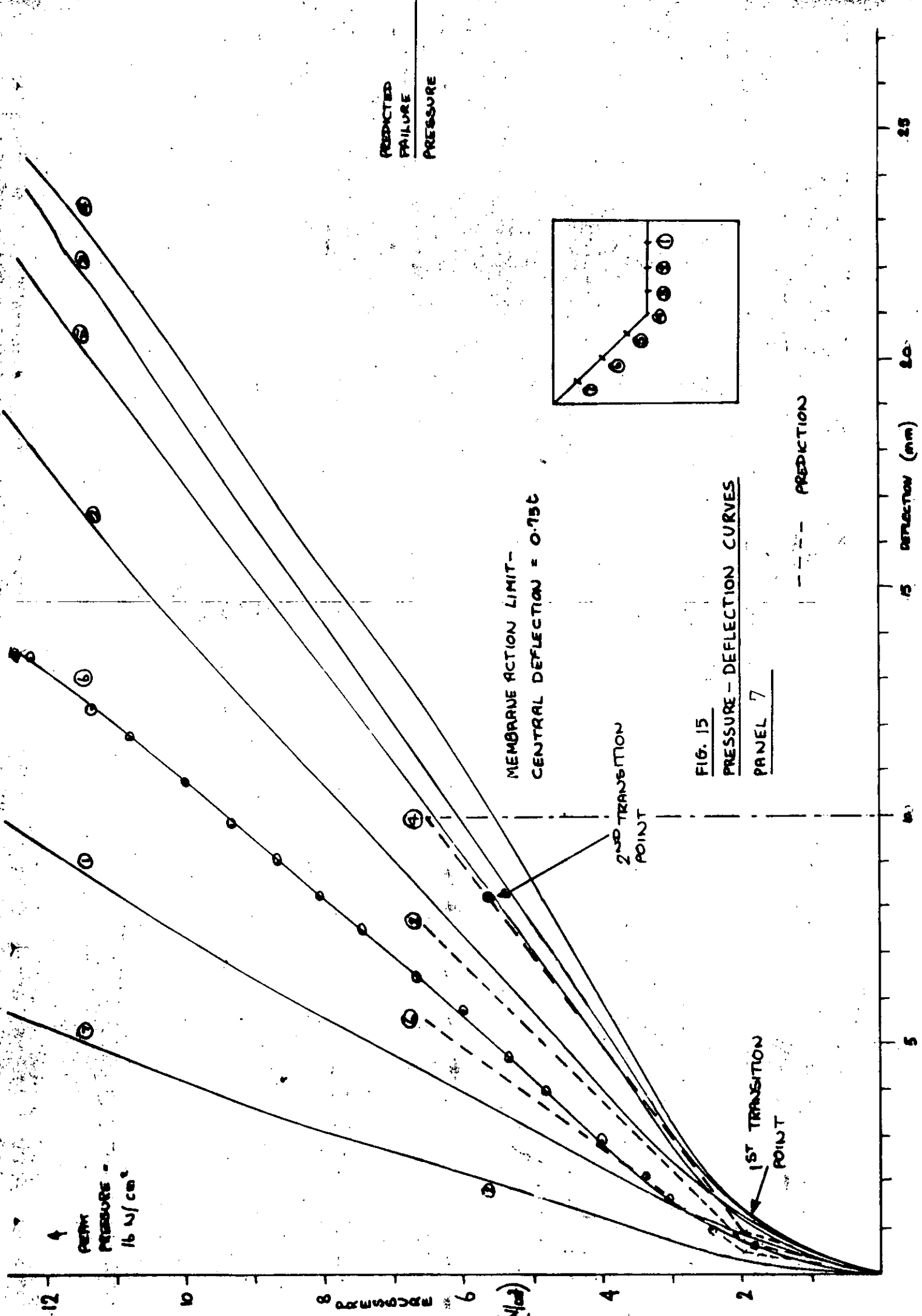
FIG. 15
PRESSURE - DEFLECTION CURVES
PANEL 7

--- PREDICTION

FIG. 16
PRESSURE - DEFLECTION CURVES
PANEL 8

CENTRAL DEFLECTION (m.m.)

FIG. 18 BEAM TESTS:—
MOMENT — DEFLECTION
DIAGRAMS

PREDICTED FAILURE MOMENT

MOMENT (Nm)

CENTRAL DEFLECTION (m.m.)

FIG. 17 BEAM TESTS:—
MOMENT — DEFLECTION
DIAGRAMS

PREDICTED FAILURE MOMENT

MOMENT (Nm)